A nonlocal operator method for finite deformation higher-order gradient elasticity

Huilong Ren, Xiaoying Zhuang, Nguyen-Thoi Trung, Timon Rabczuk

A nonlocal operator method for finite deformation higher-order gradient elasticity

Huilong Ren[a], Xiaoying Zhuang[b,c], Nguyen-Thoi Trung[d], Timon Rabczuk[d,e,*]

[a]*Institute of Structural Mechanics, Bauhaus-Universität Weimar, 99423 Weimar, Germany*
[b]*State Key Laboratory of Disaster Reduction in Civil Engineering, College of Civil Engineering,Tongji University, Shanghai 200092, China*
[c]*Institute of Continuum Mechanics, Leibniz University Hannover, Hannover, Germany*
[d]*Division of Computational Mechanics, Ton Duc Thang University, Ho Chi Minh City, Viet Nam*
[e]*Faculty of Civil Engineering, Ton Duc Thang University, Ho Chi Minh City, Viet Nam*

Abstract

We present a general finite deformation higher-order gradient elasticity theory. The governing equations of the higher-order gradient solid along with boundary conditions of various orders are derived from a variational principle using integration by parts on the surface. The objectivity of the energy functional is achieved by carefully selecting the invariants under rigid-body transformation. The third-order gradient solid theory includes more than 10.000 material parameters. However, under certain simplifications, the material parameters can be greatly reduced; down to 3. With this simplified formulation, we develop a nonlocal operator method and apply it to several numerical examples. The numerical analysis shows that the high gradient solid theory exhibits a stiffer response compared to a 'conventional' hyperelastic solid. The numerical tests also demonstrate the capability of the nonlocal operator method in solving higher-order physical problems.

Keywords: Nonlocal operator method, finite strain, second/third-gradient strain, invariant, variational principle

*Corresponding author:Timon Rabczuk, Division of Computational Mechanics, Ton Duc Thang University, Ho Chi Minh City, Viet Nam

Email address: timon.rabczuk@tdtu.edu.vn (Timon Rabczuk)

1. Introduction

Gradient theories have attracted increasing interest due to their capability of describing phenomena such as size effects, edge and skin effects as well as nonlocal effects in materials, which cannot be tackled by conventional continuum mechanics. Gradient elasticity theory introduces an internal length scale and higher-order gradients of the displacement field to account for size effects at the micro- or nano-scale. Gradient theories emerge from considerations of the microstructure in the material at micro-scale, where a mass point after homogenization is not the center of a micro-volume and the rotation of the micro-volume depends on the moment stress/couple stress as well as the Cauchy stress. The starting point of gradient elasticity theory can be traced back to Cosserat theory in 1909 [1]. A variety of gradient elasticity theories have been proposed which include Mindlin solid theory [2, 3], nonlocal elasticity [4], couple stress theory [5, 6, 7], modified couple stress [8, 9] and second-grade materials [10].

Gradient elasticity as a generalization of classical elasticity includes the contribution of strain gradients in the strain energy. Different from classical elasticity theory, such consideration enables gradient elasticity to model some interesting phenomena (such as size effect, the stress and strain effects on surface physics, nonlocal effect at micrometer/nanometer scale). Muller and Saul [11] reviewed the importance of surface and interface stress effects on thin films and nano-scaled structures, including the self-organization and elastic driven instabilities of nano-structures. Fischer etal. [12] studied the role of the surface energy and surface stress in phase-transforming nano-particles. Davydov etal. [13] showed that a continuum based on gradient elasticity with surface energy contributions can capture size effects that are observed in atomistic simulations. In Refs [14, 15, 16] , it is shown that gradient elasticity theory can circumvent stress singularities in local elasticity. Gradient elasticity is closely linked to flexoelectricity, where the strain gradient causes an electromechanical effect [17, 18, 19]. Due to the regularity property of continuum mechanics, gradient elasticity has been applied to problems with strain localization [20, 21, 22]. The micro-structure in continua also plays a crucial role in metamaterials [23]. Besides strain gradients, velocity

gradients enable a more realistic description of dispersive characteristics of the wave propagation in a nonhomogeneous medium such as polymer foams, porous materials, high-toughness ceramics [3, 24] and carbon nanotubes [25].

Second-gradient elasticity, taking into account the Hessian of the strain tensor, can be viewed as a generalization of gradient elasticity. This theory has been firstly proposed by Mindlin in 1965 [26] in order to account for cohesive force and surface-tension in solids. Beside the second-gradient term in the displacement field, Polizzotto [27, 28] studied the static/dynamic behavior of linear second-gradient elasticity with second velocity gradient inertia. Askes etal. [29, 25] showed higher order inertia models are able to realistically describe wave dispersion phenomena in a nonhomogeneous medium. Javili etal. [30] derived the governing equations and boundary conditions for third-gradient elasticity with geometrical nonlinearities from variational principles. In the derivation, the bulk and boundary (surface and curve) energies are considered as independent energy forms and three balance laws are established in their respective domains. Reiher etal. [31, 32] developed a finite third-strain gradient elasticity/elastoplasticity theory.

The higher order continuity in gradient elasticity theory imposes challenges on many numerical methods. In order to satisfy the C^1 or C^2 continuity, a variety of numerical methods have been developed, see for instance the mixed finite element method proposed in [33, 34, 35, 16], boundary element method [36], meshless methods [37, 38], isogeometric analysis (IGA) formulations [39, 40, 41, 42, 43, 44] and nonlocal operator method (NOM) [45, 46, 47]. NOM is proposed as a generalization of dual-horizon peridynamics [48, 49, 50, 51]. It uses an integral form (i.e.nonlocal operators) to replace the local partial differential operators of various orders. The nonlocal operators can be viewed as an alternative to the partial derivatives of shape functions in FEM. Combined with a variational principle or weighted residual method, NOM obtains the residual vector and tangent stiffness matrix in the same way as in FEM. There are three versions of NOM, first-order particle-based NOM [47, 52], higher order particle-based NOM [46] and higher order NOM based on numerical integration [45]. The particle-based version can be viewed as a special case of NOM with numerical integration when nodal integration is employed. NOM has been applied to the solution of

the Poisson equations in high dimensional space, von-Karman thin plate equations, fracture problems based on phase fields [46], waveguide problem in electromagnetic field [52] and gradient solid problems [45]. NOM is suitable for problems requiring higher order continuity though its application to higher order gradient elasticity has not been explored yet.

Current higher order gradient solid theory is limited to third order. Javili etal. [30] implemented the variational derivation of the third-gradient elasticity without considering the specific forms of energy. The derivation follows the setting of first Piola-Kirchhoff stress. The concrete form of third-strain gradient theory with finite deformation is proposed in [31], where the objectivity of the energy form is emphasized. However, an associated implementation is missing to our best knowledge. In this paper, we propose a different strain energy density with objectivity. The energy form is based on the second Piola-Kirchhoff stress and is invariant under rigid body transformation. The number of gradient order is extended to 5 in 2D and 3 in 3D. For the first time, the geometrical nonlinear fifth-order gradient elasticity in 2D and third-order gradient elasticity in 3D are studied by numerical experiments based on nonlocal operator method.

The content of the paper is outlined as follows. The general strain energy density for large deformations is proposed for the fourth-order gradient elasticity in section 2. In Section 3, we derive the governing equations and the associated boundary conditions for the third-order gradient elasticity by using variational principles and exploiting integration by parts on surfaces. In section 4, the framework of the particle-based nonlocal operator method is briefly summarized and its implementation for solving higher order gradient solids presented. In section 5, several representative numerical tests, including a point displacement load, point force load and the influence of the length scale in linear/nonlinear gradient elasticity, are presented to study the physical response of higher order gradient elasticity. Finally, we conclude our manuscript in section 6.

2. Higher order gradient solid with finite deformation

Let us denote the material coordinates (in the initial configuration Ω) by $\boldsymbol{X}$, the spatial coordinates (in the current configuration Ω_t) by $\boldsymbol{x}$ and the displacement field by $\boldsymbol{u} := \boldsymbol{x} - \boldsymbol{X}$.

The deformation gradient $\boldsymbol{F}$, right Cauchy Green tensor $\boldsymbol{C}$ and Green-Lagrange strain tensor $\boldsymbol{E}$ are written as

$$\boldsymbol{F} = \frac{\partial \boldsymbol{x}}{\partial \boldsymbol{X}} = \nabla \boldsymbol{x} = \nabla \boldsymbol{u} + \boldsymbol{I} \tag{1}$$

$$\boldsymbol{C} = \boldsymbol{F}^T \cdot \boldsymbol{F}, \boldsymbol{E} = \frac{1}{2}(\boldsymbol{C} - \boldsymbol{I}) \tag{2}$$

where $\boldsymbol{I}$ is the identity matrix and $\nabla \square = \frac{\partial \square}{\partial \boldsymbol{X}}$. The principle of frame indifference requires the quantity remain invariant under rigid body transformation $\boldsymbol{x}' = \boldsymbol{Q}(t)\boldsymbol{x} + \boldsymbol{c}(t)$ where $\boldsymbol{c}(t)$ is the rigid translation vector, $\boldsymbol{Q}(t)$ the (orthogonal) rotation matrix satisfying $\boldsymbol{Q}\boldsymbol{Q}^T = \boldsymbol{Q}^T\boldsymbol{Q} = \boldsymbol{I}$. Vectors and second-order tensors are objective if they are related by the rotation tensor as

$$\boldsymbol{u}' = \boldsymbol{Q} \cdot \boldsymbol{u} \tag{3}$$

$$\boldsymbol{T}' = \boldsymbol{Q} \cdot \boldsymbol{T} \cdot \boldsymbol{Q}^T \tag{4}$$

The deformation gradient under rigid body transformation is related by

$$\boldsymbol{F}' = \frac{\partial \boldsymbol{x}'}{\partial \boldsymbol{X}} = \frac{\partial \boldsymbol{x}'}{\partial \boldsymbol{x}} \cdot \frac{\partial \boldsymbol{x}}{\partial \boldsymbol{X}} = \boldsymbol{Q} \cdot \boldsymbol{F} \tag{5}$$

Quantities are invariant if they remain unchanged by the rigid body transformation. Apparently, the right Cauchy tensor is invariant as $\boldsymbol{C}' = \boldsymbol{F}'^T\boldsymbol{F}' = \boldsymbol{F}^T\boldsymbol{Q}^T\boldsymbol{Q}\boldsymbol{F} = \boldsymbol{F}^T\boldsymbol{F} = \boldsymbol{C}$. Let $\boldsymbol{F}_{,i} := \frac{\partial \boldsymbol{F}}{\partial X_i}$ denote the partial derivative of $\boldsymbol{F}$ with respect to X_i. The derivative of $\boldsymbol{F}'$ and $\boldsymbol{Q}$ can be written as

$$\boldsymbol{F}'_{,i} = \boldsymbol{Q}_{,i}\boldsymbol{F} + \boldsymbol{Q}\boldsymbol{F}_{,i} \tag{6}$$

$$\boldsymbol{Q}^T_{,i}\boldsymbol{Q} + \boldsymbol{Q}^T\boldsymbol{Q}_{,i} = 0 \tag{7}$$

The gradient of $\boldsymbol{C}'$ can be derived as

$$\begin{aligned}
\boldsymbol{C}'_{,i} &= (\boldsymbol{F}'^T\boldsymbol{F}')_{,i} = \boldsymbol{F}'^T_{,i}\boldsymbol{F}' + \boldsymbol{F}'^T\boldsymbol{F}'_{,i} \\
&= (\boldsymbol{F}^T\boldsymbol{Q}^T_{,i} + \boldsymbol{F}^T_{,i}\boldsymbol{Q}^T)\boldsymbol{Q}\boldsymbol{F} + \boldsymbol{F}^T\boldsymbol{Q}^T(\boldsymbol{Q}_{,i}\boldsymbol{F} + \boldsymbol{Q}\boldsymbol{F}_{,i}) \\
&= \boldsymbol{F}^T\boldsymbol{Q}^T_{,i}\boldsymbol{Q}\boldsymbol{F} + \boldsymbol{F}^T_{,i}\boldsymbol{Q}^T\boldsymbol{Q}\boldsymbol{F} + \boldsymbol{F}^T\boldsymbol{Q}^T\boldsymbol{Q}_{,i}\boldsymbol{F} + \boldsymbol{F}^T\boldsymbol{Q}^T\boldsymbol{Q}\boldsymbol{F}_{,i} \\
&= -\boldsymbol{F}^T\boldsymbol{Q}^T\boldsymbol{Q}_{,i}\boldsymbol{F} + \boldsymbol{F}^T\boldsymbol{Q}^T\boldsymbol{Q}_{,i}\boldsymbol{F} + \boldsymbol{F}^T\boldsymbol{F}_{,i} + \boldsymbol{F}^T_{,i}\boldsymbol{F} \\
&= (\boldsymbol{F}^T\boldsymbol{F})_{,i} = \boldsymbol{C}_{,i}.
\end{aligned} \tag{8}$$

Therefore $\nabla \boldsymbol{C}$ is invariant. Note that $\nabla \boldsymbol{F}$ is neither objective nor invariant since

$$\boldsymbol{F}'_{,i} = (\boldsymbol{Q}\boldsymbol{F})_{,i} = \boldsymbol{Q}_{,i}\boldsymbol{F} + \boldsymbol{Q}\boldsymbol{F}_{,i} \neq \boldsymbol{F}_{,i} \tag{9}$$

$$\nabla \boldsymbol{F} \vdots \nabla \boldsymbol{F} = \sum_i \boldsymbol{F}_{,i} : \boldsymbol{F}_{,i} \neq \sum_i \boldsymbol{F}'_{,i} : \boldsymbol{F}'_{,i}. \tag{10}$$

Hence $\nabla \boldsymbol{F}$ cannot be used directly to define the energy density. However, the invariant property makes $\nabla \boldsymbol{C}$ a good choice. Different orders of strain gradient can be written as

$$\boldsymbol{H} = \frac{\partial \boldsymbol{E}}{\partial \boldsymbol{X}} = \nabla \boldsymbol{E} = \frac{1}{2}(\boldsymbol{F}^T \nabla \boldsymbol{F} + \nabla \boldsymbol{F}^T \boldsymbol{F}) \tag{11}$$

for the first gradient strain tensor,

$$\boldsymbol{G} = \frac{\partial \boldsymbol{H}}{\partial \boldsymbol{X}} = \frac{\partial^2 \boldsymbol{E}}{\partial \boldsymbol{X}^2} = \nabla^2 \boldsymbol{E} \tag{12}$$

for the second-gradient strain tensor, and

$$\boldsymbol{L} = \frac{\partial \boldsymbol{G}}{\partial \boldsymbol{X}} = \frac{\partial^3 \boldsymbol{E}}{\partial \boldsymbol{X}^3} = \nabla^3 \boldsymbol{E} \tag{13}$$

for the third-gradient strain tensor and with $\nabla^n = \underbrace{\nabla \otimes ... \otimes \nabla}_{n\ times}$. Most 'computational' contributions focus on applications with small strain gradients. In this case, strain gradients of different orders are decoupled. Note that the expression in $\boldsymbol{L}$ contains derivatives ranging from $\nabla \boldsymbol{u}$ to $\nabla^4 \boldsymbol{u}$, which is due to geometric nonlinearities arising from finite deformation. The exact forms of $\boldsymbol{L}, \boldsymbol{G}$ can be derived with Mathematica. It can be verified that $\boldsymbol{C}, \boldsymbol{E}, \boldsymbol{H}, \boldsymbol{G}, \boldsymbol{L}$ are invariants under rigid body translations and rotations. Thus, these quantities can be used to define the stresses and generalized stresses

$$S_{ij} = \mathbb{D}_{ijkl} E_{kl} \text{ with } \mathbb{D}_{ijkl} = \frac{\partial S_{ij}}{\partial E_{kl}} \tag{14a}$$

$$R_{ijk} = \mathbb{E}_{ijklmn} H_{lmn} \text{ with } \mathbb{E}_{ijklmn} = \frac{\partial R_{ijk}}{\partial H_{lmn}} \tag{14b}$$

$$Q_{ijkl} = \mathbb{F}_{ijklmnst} G_{mnst} \text{ with } \mathbb{F}_{ijklmnst} = \frac{\partial Q_{ijkl}}{\partial G_{mnst}} \tag{14c}$$

$$P_{ijklm} = \mathbb{G}_{ijklm\alpha\beta\gamma\eta\delta} L_{\alpha\beta\gamma\eta\delta} \text{ with } \mathbb{G}_{ijklm\alpha\beta\gamma\eta\delta} = \frac{\partial P_{ijklm}}{\partial L_{\alpha\beta\gamma\eta\delta}} \tag{14d}$$

Eq.14a has the exact form of the Saint Venant–Kirchhoff model. R_{ijk}, Q_{ijkl} and P_{ijklm} are defined as the generalization of the Saint Venant-Kirchhoff model.

The strain energy density in the initial configuration can be assumed as

$$\phi = \frac{1}{2}(S_{ij}E_{ij} + R_{ijk}H_{ijk} + Q_{ijkl}G_{ijkl} + P_{ijklm}L_{ijklm}) \tag{15}$$

$$= \frac{1}{2}(E_{ij}\mathbb{D}_{ijkl}E_{kl} + H_{ijk}\mathbb{E}_{ijklmn}H_{lmn} + G_{ijkl}\mathbb{F}_{ijklmnst}G_{mnst} + L_{ijklm}\mathbb{G}_{ijklm\alpha\beta\gamma\eta\delta}L_{\alpha\beta\gamma\eta\delta}) \tag{16}$$

where $\mathbb{D}$ is a 4th-order tensor, $\mathbb{E}$ a 6th-order tensor, $\mathbb{F}$ an 8th-order tensor and $\mathbb{G}$ a 10th-order tensor. The second Piola-Kirchhoff stress is work conjugate to the Green-Lagrange strain [53, 54]. Therefore, the generalized second Piola-Kirchhoff stresses define the strain energy density in the initial configuration and are objective under any rigid body transformations. The strain energy density, given by Eq.16, is among the most simplified quadratic energy functionals. This energy functional is required to be positive, which can be satisfied provided that the material tensors $\mathbb{D}, \mathbb{E}, \mathbb{F}$ and $\mathbb{G}$ are positive definite. For an n dimensional space, a kth-order tensor has n^k entries, for example $\mathbb{G}$ has $2^{10} = 1\,024$ elements in 2D and $3^{10} = 59\,049$ elements in 3D. However, when symmetry conditions are exploited, the number of elements can be greatly reduced. We discussed the symmetry of a 6th-order tensor in Appendix A and in Voigt notation in Appendix B. For a third-order gradient solid, there are thousands of material parameters to be determined, which are complicated to resolve experimentally. For simplicity, we introduce only three material length scales.

$$\phi(\boldsymbol{E}, \nabla\boldsymbol{E}, \nabla^2\boldsymbol{E}, \nabla^3\boldsymbol{E}) = \frac{1}{2}\Big(\boldsymbol{S} : \boldsymbol{E} + l_1^2\nabla\boldsymbol{S}\vdots\nabla\boldsymbol{E} + l_2^4\nabla^2\boldsymbol{S} \cdot^{(4)} \nabla^2\boldsymbol{E} + l_3^6\nabla^3\boldsymbol{S} \cdot^{(5)} \nabla^3\boldsymbol{E}\Big) \tag{17}$$

where $\cdot^{(k)}$ is the generalization of the inner product, for example, $\cdot^{(1)} = \cdot, \cdot^{(2)} =:, \cdot^{(3)} = \vdots$, and the stresses can be written as

$$\boldsymbol{S} = \mathbb{D} : \boldsymbol{E} \tag{18a}$$

$$\boldsymbol{R} = \nabla\boldsymbol{S} \tag{18b}$$

$$\boldsymbol{Q} = \nabla^2\boldsymbol{S} \tag{18c}$$

$$\boldsymbol{P} = \nabla^3\boldsymbol{S}. \tag{18d}$$

The total internal strain energy in the domain can be expressed as

$$\mathcal{F}_{int} = \int_{\Omega} \phi(\boldsymbol{E}, \nabla \boldsymbol{E}, \nabla^2 \boldsymbol{E}, \nabla^3 \boldsymbol{E}) \tag{19}$$

We recall that Ω is the initial configuration. Here we used $\int_{\Omega}\{\cdot\} := \int_{\Omega}\{\cdot\}\ \mathbf{d}V$. When small deformations are assumed, the Green-Lagrange strain and second Piola-Kirchhoff stress degenerate to the linear strain and Cauchy stress tensor:

$$\boldsymbol{E} \to \varepsilon = \frac{1}{2}\Big((\nabla \boldsymbol{u})^T + \nabla \boldsymbol{u}\Big) \tag{20}$$

$$\boldsymbol{S} \to \sigma = \mathbb{D} : \varepsilon \tag{21}$$

Then Eq.17 can be written as

$$\phi(\varepsilon, \nabla\varepsilon, \nabla^2\varepsilon, \nabla^3\varepsilon) = \frac{1}{2}(\sigma : \varepsilon + l_1^2 \nabla\sigma \vdots \nabla\varepsilon + l_2^4 \nabla^2\sigma \cdot^{(4)} \nabla^2\varepsilon + l_3^6 \nabla^3\sigma \cdot^{(5)} \nabla^3\varepsilon) \tag{22}$$

Based on the simplified higher gradient elasticity in Eq.17, the general nth-gradient elasticity can be written as

$$\phi(\boldsymbol{E}, \nabla \boldsymbol{E}, \nabla^2 \boldsymbol{E}, ..., \nabla^n \boldsymbol{E}) = \frac{1}{2}\Big(\boldsymbol{S} : \boldsymbol{E} + \sum_{k=1}^{n} (l_k)^{2k}\, \nabla^k \boldsymbol{S} \cdot^{(k+2)} \nabla^k \boldsymbol{E}\Big) \tag{23}$$

where l_k is the internal length scale of kth-order. We employ E^n elasticity ($n = 0, 1, 2, 3, 4, 5$) to abbreviate the nth-gradient hyperelasticity theory wherein $\nabla^n \boldsymbol{E}$ is used to define the energy density functional. Accordingly, the conventional hyperelasticity is denoted by E^0 elasticity, gradient elasticity is abbreviated by E^1 elasticity and the second-gradient elasticity by E^2 elasticity. The highest order of the energy form of E^n-elasticity is $(n+1)$, while that of the strong form is $2(n+1)$. The highest order of gradient elasticity we implemented is the E^5 elasticity in 2D. For E^5 elasticity, the governing equations are a set of 12th-order nonlinear partial differential equations (PDEs).

3. Governing equations of second-gradient solid

3.1. Integration by parts on close surface

Before delving into the variational derivation of second-gradient solids, we briefly review the integration by parts in domains and on surfaces using the following abbreviations

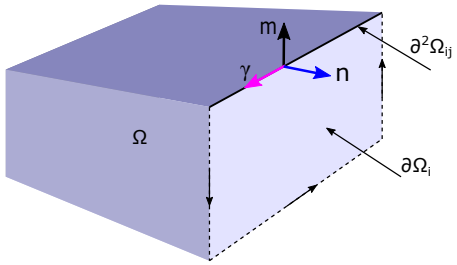

Figure 1: Domain with piecewise smooth surfaces; $\boldsymbol{n}$ is the outward unit normal direction of surface boundary $\partial\Omega$, $\boldsymbol{\gamma}$ is the tangent direction of line boundary $\partial^2\Omega_{ij}$, $\boldsymbol{m} = \boldsymbol{\gamma} \times \boldsymbol{n}$ is the outward normal unit vector of line boundary.

$\int_\Omega\{\cdot\} := \int_\Omega\{\cdot\}\ \mathbf{d}V$ and $\int_{\partial\Omega}\{\cdot\} := \int_{\partial\Omega}\{\cdot\}\ \mathbf{d}\Gamma$. The integration by parts for tensor fields in Ω is

$$\int_\Omega \boldsymbol{S} : \nabla\boldsymbol{u} = \int_{\partial\Omega} \boldsymbol{n}\cdot\boldsymbol{S}\cdot\boldsymbol{u} - \int_\Omega \nabla\cdot\boldsymbol{S}\cdot\boldsymbol{u} \tag{24}$$

where $\boldsymbol{S}$ is the second-order tensor field and $\boldsymbol{u}$ is the vector field.

According to Refs [55, 56], the integration by parts under the assumption of smooth surfaces can be expressed as

$$\int_{\partial\Omega} \boldsymbol{S} : \nabla\boldsymbol{u} = \int_{\partial\Omega} \boldsymbol{S} : \nabla_n\boldsymbol{u} + \int_{\partial\Omega} \boldsymbol{S} : \nabla_t\boldsymbol{u} = \int_{\partial\Omega} \Big(\boldsymbol{S} : \nabla_n\boldsymbol{u} + (g\boldsymbol{n}\cdot\boldsymbol{S} - \nabla_t\cdot\boldsymbol{S})\cdot\boldsymbol{u}\Big) \tag{25}$$

where $g = \nabla_t\cdot\boldsymbol{n}$ is the Gauss curvature, ∇_t and ∇_n are the tangential and normal gradient

$$\nabla_t = (1 - \boldsymbol{n}\boldsymbol{n}^T)\cdot\nabla, \quad \nabla_n = \boldsymbol{n}\boldsymbol{n}^T\cdot\nabla \tag{26}$$

In the above derivation, $\nabla\boldsymbol{u}$ needs to be divided into the tangential and normal parts with respect to the surface, i.e.$\nabla\boldsymbol{u} = \nabla_t\boldsymbol{u} + \nabla_n\boldsymbol{u}$. For the case of piecewise smooth surfaces shown in Fig.1, the boundary term should be considered explicitly,

$$\int_{\partial\Omega} \boldsymbol{S} : \nabla\boldsymbol{u} = \int_{\partial\Omega} \Big(\boldsymbol{S} : \nabla_n\boldsymbol{u} + (g\boldsymbol{n}\cdot\boldsymbol{S} - \nabla_t\cdot\boldsymbol{S})\cdot\boldsymbol{u}\Big) + \int_{\partial^2\Omega} \boldsymbol{m}\cdot\boldsymbol{S}\cdot\boldsymbol{u} \tag{27}$$

where $\boldsymbol{m}$ is the outward normal direction of $\partial\Omega$ in the tangent plane defined by $\boldsymbol{n}$. If both $\boldsymbol{S}$ and $\nabla\boldsymbol{u}$ are defined based on the tangent space of the surface, i.e. $\boldsymbol{n}\cdot\boldsymbol{S} = \boldsymbol{0}$ and $\nabla_n\boldsymbol{u} = \boldsymbol{0}$, the integration by parts on surface is the same as Eq.24.

3.2. Variational derivation of second-gradient solid

In this paper, we only consider the higher order bulk energy. For the boundary (surface and curve) energies, the reader is referred to [30] for more details. The second-gradient solid for linear elasticity with second velocity gradient inertia can be found in [27, 28]. Let $\phi := \phi(\boldsymbol{u}, \nabla\boldsymbol{u}, \nabla^2\boldsymbol{u}, \nabla^3\boldsymbol{u})$ denote the internal energy density of a second-gradient solid (E^2 elasticity). The variation of the internal energy in Ω is then given by

$$\begin{aligned}\delta\mathcal{F}_{int} &= \int_\Omega \underbrace{\frac{\partial\phi}{\partial\boldsymbol{u}}}_{\boldsymbol{b}}\cdot\delta\boldsymbol{u} + \underbrace{\frac{\partial\phi}{\partial\nabla\boldsymbol{u}}}_{\boldsymbol{S}_1} : \nabla\delta\boldsymbol{u} + \underbrace{\frac{\partial\phi}{\partial\nabla^2\boldsymbol{u}}}_{\boldsymbol{S}_2} \vdots \nabla^2\delta\boldsymbol{u} + \underbrace{\frac{\partial\phi}{\partial\nabla^3\boldsymbol{u}}}_{\boldsymbol{S}_3} :: \nabla^3\delta\boldsymbol{u} \\ &= \int_\Omega \underbrace{\boldsymbol{b}\cdot\delta\boldsymbol{u}}_{p1} + \underbrace{\boldsymbol{S}_1 : \nabla\delta\boldsymbol{u}}_{p2} + \underbrace{\boldsymbol{S}_2 \vdots \nabla^2\delta\boldsymbol{u}}_{p3} + \underbrace{\boldsymbol{S}_3 :: \nabla^3\delta\boldsymbol{u}}_{p4}\end{aligned} \tag{28}$$

where $\boldsymbol{b}$ can be viewed as the body force density, $\boldsymbol{S}_i$ denotes the work conjugate to $\nabla^i\boldsymbol{u}, (i = 1, 2, 3)$ and $\boldsymbol{S}_i$ the general stress defined in the initial configuration:

$$\boldsymbol{S}_3 = \frac{\partial\phi}{\partial\nabla^3\boldsymbol{u}} = \frac{\partial\phi}{\partial\nabla^2\boldsymbol{E}} :: \frac{\partial\nabla^2\boldsymbol{E}}{\partial\nabla^3\boldsymbol{u}} \tag{29a}$$

$$\boldsymbol{S}_2 = \frac{\partial\phi}{\partial\nabla^2\boldsymbol{u}} = \frac{\partial\phi}{\partial\nabla\boldsymbol{E}} \vdots \frac{\partial\nabla\boldsymbol{E}}{\partial\nabla^2\boldsymbol{u}} + \frac{\partial\phi}{\partial\nabla^2\boldsymbol{E}} :: \frac{\partial\nabla^2\boldsymbol{E}}{\partial\nabla^2\boldsymbol{u}} \tag{29b}$$

$$\boldsymbol{S}_1 = \frac{\partial\phi}{\partial\nabla\boldsymbol{u}} = \frac{\partial\phi}{\partial\boldsymbol{E}} : \frac{\partial\boldsymbol{E}}{\partial\nabla\boldsymbol{u}} + \frac{\partial\phi}{\partial\nabla\boldsymbol{E}} \vdots \frac{\partial\nabla\boldsymbol{E}}{\partial\nabla\boldsymbol{u}} + \frac{\partial\phi}{\partial\nabla^2\boldsymbol{E}} :: \frac{\partial\nabla^2\boldsymbol{E}}{\partial\nabla\boldsymbol{u}} \tag{29c}$$

where $\boldsymbol{E}, \nabla\boldsymbol{E}, \nabla^2\boldsymbol{E}$ have the forms

$$\boldsymbol{E} = \frac{1}{2}\Big(\nabla\boldsymbol{u}^T + \nabla\boldsymbol{u} + \nabla\boldsymbol{u}^T\nabla\boldsymbol{u}\Big) \tag{30a}$$

$$\nabla\boldsymbol{E} = \frac{1}{2}\Big(\nabla(\nabla\boldsymbol{u})^T + \nabla^2\boldsymbol{u} + \nabla(\nabla\boldsymbol{u})^T\nabla\boldsymbol{u} + \nabla\boldsymbol{u}^T\nabla^2\boldsymbol{u}\Big) \tag{30b}$$

$$\begin{aligned}\nabla^2\boldsymbol{E} = \frac{1}{2}\Big(&\nabla^2(\nabla\boldsymbol{u})^T + \nabla^3\boldsymbol{u} + \nabla^2(\nabla\boldsymbol{u})^T\nabla\boldsymbol{u} + \\ &\nabla(\nabla\boldsymbol{u})^T\nabla^2\boldsymbol{u} + \nabla(\nabla\boldsymbol{u})^T\nabla^2\boldsymbol{u} + (\nabla\boldsymbol{u})^T\nabla^3\boldsymbol{u}\Big)\end{aligned} \tag{30c}$$

Obviously, higher order strain gradients contain a low order gradient due to the existence of a geometric nonlinearity. The explicit form of $\boldsymbol{S}_1, \boldsymbol{S}_2, \boldsymbol{S}_3$ can be derived by mathematical software such as Mathematica. Since the order of the derivatives is reduced by one each time when applying integration by parts, we integrate the terms from high order to low order so that the derived low order term with the existing low order term can be handled together.

In other words, the term with the third-order gradient is firstly integrated by parts, then the second-order gradient term and the accumulated gradient terms at last.

The $p4$ part in Eq.28 via Eq.24 can be written as

$$\begin{aligned}\int_\Omega \boldsymbol{S}_3 :: \nabla^3\delta\boldsymbol{u} &= \int_{\partial\Omega} \boldsymbol{n}\cdot\boldsymbol{S}_3 \vdots \nabla^2\delta\boldsymbol{u} + \int_\Omega -\nabla\cdot\boldsymbol{S}_3 \vdots \nabla^2\delta\boldsymbol{u} \\ &= \int_{\partial\Omega} \underbrace{\boldsymbol{n}\cdot\boldsymbol{S}_3 \vdots \nabla_t(\nabla\delta\boldsymbol{u})}_{p7} + \int_{\partial\Omega} \underbrace{\boldsymbol{n}\cdot\boldsymbol{S}_3 \vdots \nabla_n(\nabla\delta\boldsymbol{u})}_{p8} + \int_\Omega \underbrace{-\nabla\cdot\boldsymbol{S}_3 \vdots \nabla^2\delta\boldsymbol{u}}_{p6}\end{aligned} \tag{31}$$

The $p7$ part in Eq.31 is obtained via integration by parts on surface

$$\begin{aligned}\int_{\partial\Omega} \boldsymbol{n}\cdot\boldsymbol{S}_3 \vdots \nabla_t(\nabla\delta\boldsymbol{u}) &= \int_{\partial\Omega} \underbrace{\Big(g\boldsymbol{n}\cdot(\boldsymbol{n}\cdot\boldsymbol{S}_3) - \nabla_t\cdot(\boldsymbol{n}\cdot\boldsymbol{S}_3)\Big)}_{\boldsymbol{V}_1} : \nabla\delta\boldsymbol{u} \\ &= \int_{\partial\Omega} \underbrace{\boldsymbol{V}_1 : \nabla\delta\boldsymbol{u}}_{p9}\end{aligned} \tag{32}$$

In above derivation, we abbreviate the long expression as $\boldsymbol{V}_1$. Based on Eq.25, the $p9$ part reads

$$\int_{\partial\Omega} \boldsymbol{V}_1 : \nabla\delta\boldsymbol{u} = \int_{\partial\Omega} \boldsymbol{V}_1 : \nabla_n\delta\boldsymbol{u} + (g\boldsymbol{n}\cdot\boldsymbol{V}_1 - \nabla_t\cdot\boldsymbol{V}_1)\cdot\delta\boldsymbol{u} \tag{33}$$

Hence, $p4$ has the form

$$\int_\Omega \boldsymbol{S}_3 :: \nabla^3\delta\boldsymbol{u} = \int_{\partial\Omega} \boldsymbol{V}_1 : \nabla\delta\boldsymbol{u} + \int_{\partial\Omega} \underbrace{\boldsymbol{n}\cdot\boldsymbol{S}_3 \vdots \nabla_n(\nabla\delta\boldsymbol{u})}_{p8} + \int_\Omega \underbrace{-\nabla\cdot\boldsymbol{S}_3 \vdots \nabla^2\delta\boldsymbol{u}}_{p6} \tag{34}$$

The $p6$ term has the same form as part $p3$ in Eq.28 and it can be estimated that a new

surface term similar to $p9$ part will arise. The summation of p_3, p_6, p_9 can be written as

$$\begin{aligned}
&\int_\Omega \boldsymbol{S}_2 \vdots \nabla^2 \delta\boldsymbol{u} - \nabla\cdot\boldsymbol{S}_3 \vdots \nabla^2\delta\boldsymbol{u} + \int_{\partial\Omega} \boldsymbol{V}_1 : \nabla\delta\boldsymbol{u} = \underbrace{\int_\Omega (\boldsymbol{S}_2 - \nabla\cdot\boldsymbol{S}_3)\vdots\nabla^2\delta\boldsymbol{u}}_{by\ Eq.24} + \int_{\partial\Omega} \boldsymbol{V}_1 : \nabla\delta\boldsymbol{u} \\
&= \underbrace{\int_{\partial\Omega} \boldsymbol{n}\cdot(\boldsymbol{S}_2 - \nabla\cdot\boldsymbol{S}_3) : \nabla\delta\boldsymbol{u} + \int_{\partial\Omega} \boldsymbol{V}_1 : \nabla\delta\boldsymbol{u}}_{by\ Eq.25} - \int_\Omega \nabla\cdot(\boldsymbol{S}_2 - \nabla\cdot\boldsymbol{S}_3) : \nabla\delta\boldsymbol{u} \\
&= \int_{\partial\Omega} \underbrace{(g\boldsymbol{n}\cdot\boldsymbol{V}_1 - \nabla_t\cdot\boldsymbol{V}_1 + g\boldsymbol{n}\cdot(\boldsymbol{n}\cdot(\boldsymbol{S}_2 - \nabla\cdot\boldsymbol{S}_3)) - \nabla_t\cdot(\boldsymbol{n}\cdot(\boldsymbol{S}_2 - \nabla\cdot\boldsymbol{S}_3)))}_{\boldsymbol{V}_2}\cdot\delta\boldsymbol{u} \\
&+ \int_{\partial\Omega} (\boldsymbol{V}_1 + \boldsymbol{n}\cdot(\boldsymbol{S}_2 - \nabla\cdot\boldsymbol{S}_3)) : \nabla_n\delta\boldsymbol{u} + \int_\Omega \underbrace{-\nabla\cdot(\boldsymbol{S}_2 - \nabla\cdot\boldsymbol{S}_3) : \nabla\delta\boldsymbol{u}}_{p10} \\
&= \int_{\partial\Omega} \boldsymbol{V}_2\cdot\delta\boldsymbol{u} + \int_{\partial\Omega} (\boldsymbol{V}_1 + \boldsymbol{n}\cdot(\boldsymbol{S}_2 - \nabla\cdot\boldsymbol{S}_3)) : \nabla_n\delta\boldsymbol{u} + \int_\Omega -\nabla\cdot(\boldsymbol{S}_2 - \nabla\cdot\boldsymbol{S}_3) : \nabla\delta\boldsymbol{u} \quad (35a)
\end{aligned}$$

In the above derivation, the long expression in the second line is abbreviated as $\boldsymbol{V}_2$. Both integration by parts in the domain and integration by parts on the surface are used in the derivation.

The gradient order of $p10$ is identical to that in the $p2$ part. For simplicity, the integration by parts of $p10 + p2$ is

$$\int_\Omega \underbrace{(\boldsymbol{S}_1 - \nabla\cdot(\boldsymbol{S}_2 - \nabla\cdot\boldsymbol{S}_3))}_{\boldsymbol{S}_4} : \nabla\delta\boldsymbol{u} = \int_{\partial\Omega} \boldsymbol{n}\cdot\boldsymbol{S}_4\cdot\delta\boldsymbol{u} - \int_\Omega \nabla\cdot\boldsymbol{S}_4\cdot\delta\boldsymbol{u} \tag{36}$$

By using integration by parts in Eq.24 and Eq.25 several times, the variation of the internal energy can be finally written as

$$\begin{aligned}
\delta\mathcal{F}_{int} &= \int_\Omega (\boldsymbol{b} - \nabla\cdot\boldsymbol{S}_4)\cdot\delta\boldsymbol{u} + \int_{\partial\Omega} (\boldsymbol{V}_1 + \boldsymbol{n}\cdot(\boldsymbol{S}_2 - \nabla\cdot\boldsymbol{S}_3)) : \nabla_n\delta\boldsymbol{u} \\
&\quad + \int_{\partial\Omega} \boldsymbol{V}_2\cdot\delta\boldsymbol{u} + \int_{\partial\Omega} \boldsymbol{n}\cdot\boldsymbol{S}_4\cdot\delta\boldsymbol{u} + \int_{\partial\Omega} \boldsymbol{n}\cdot\boldsymbol{S}_3\vdots\nabla_n(\nabla\delta\boldsymbol{u}) \qquad (37) \\
&= \int_\Omega (\boldsymbol{b} - \nabla\cdot\boldsymbol{S}_4)\cdot\delta\boldsymbol{u} + \int_{\partial\Omega} (\boldsymbol{V}_2 + \boldsymbol{n}\cdot\boldsymbol{S}_4)\cdot\delta\boldsymbol{u} \\
&\quad + \int_{\partial\Omega} (\boldsymbol{V}_1 + \boldsymbol{n}\cdot(\boldsymbol{S}_2 - \nabla\cdot\boldsymbol{S}_3)) : \nabla_n\delta\boldsymbol{u} + \int_{\partial\Omega} \boldsymbol{n}\cdot\boldsymbol{S}_3\vdots\nabla_n(\nabla\delta\boldsymbol{u}) \qquad (38)
\end{aligned}$$

where

$$\boldsymbol{S}_4 = \boldsymbol{S}_1 - \nabla \cdot (\boldsymbol{S}_2 - \nabla \cdot \boldsymbol{S}_3) \tag{39a}$$

$$\boldsymbol{V}_1 = g\boldsymbol{n} \cdot (\boldsymbol{n} \cdot \boldsymbol{S}_3) - \nabla_t \cdot (\boldsymbol{n} \cdot \boldsymbol{S}_3) \tag{39b}$$

$$\boldsymbol{V}_2 = g\boldsymbol{n} \cdot \boldsymbol{V}_1 - \nabla_t \cdot \boldsymbol{V}_1 + g\boldsymbol{n} \cdot (\boldsymbol{n} \cdot (\boldsymbol{S}_2 - \nabla \cdot \boldsymbol{S}_3)) - \nabla_t \cdot (\boldsymbol{n} \cdot (\boldsymbol{S}_2 - \nabla \cdot \boldsymbol{S}_3)) \tag{39c}$$

In Eq.38, we used $\partial\Omega$ to denote the boundaries, which should be tailored based on the actual boundary conditions. The variation of the internal energy yields the work-conjugate pairs on the boundaries. The expression for $\boldsymbol{V}_2$ describes the contribution from the curvature related terms (e.g. curvature and curvature gradient on surface) as well as the generalized stresses of different orders. The contribution from the surface curvature indicates that the gradient effect or nonlocal effect of the solid may be significant at the 'micro'-scale, where the surface-to-volume ratio is much larger compared to the macro scale and the surface curvature for small-scale objects is huge. This relation is consistent with the fact that the strength of a material at micro-scale is much larger than that at macro-scale.

For the gradient elasticity, the boundary conditions may contain essential boundary conditions such as translation, the gradient of the translation and force boundary conditions like stress and couple stress. The gradient of the translation is similar to the prescribed rotation on the boundary in plate/shell theory, while the couple stress is the work conjugate to the gradient of the translation.

Based on the boundary work-conjugate pairs in the variation of the internal energy, the external energy can be constructed as

$$\begin{aligned}\mathcal{F}_{ext} = &\int_{\partial\Omega_D^0} \boldsymbol{P} \cdot (\boldsymbol{u} - \bar{\boldsymbol{u}}) + \int_{\partial\Omega_N^0} \bar{\boldsymbol{P}} \cdot \boldsymbol{u} \\ &+ \int_{\partial\Omega_D^1} \boldsymbol{Q} : (\nabla_n \boldsymbol{u} - \overline{\nabla_n \boldsymbol{u}}) + \int_{\partial\Omega_N^1} \bar{\boldsymbol{Q}} : \nabla_n \boldsymbol{u} \\ &+ \int_{\partial\Omega_D^2} \boldsymbol{R} \vdots (\nabla_n \nabla \boldsymbol{u} - \overline{\nabla_n \nabla \boldsymbol{u}}) + \int_{\partial\Omega_N^2} \bar{\boldsymbol{R}} \vdots \nabla_n \nabla \boldsymbol{u}\end{aligned} \tag{40}$$

where $\boldsymbol{P} = (\boldsymbol{V}_2 + \boldsymbol{n} \cdot \boldsymbol{S}_4), \boldsymbol{Q} = (\boldsymbol{V}_1 + \boldsymbol{n} \cdot (\boldsymbol{S}_2 - \nabla \cdot \boldsymbol{S}_3)), \boldsymbol{R} = \boldsymbol{n} \cdot \boldsymbol{S}_3$, $\partial\Omega_D^i, \partial\Omega_N^i, (i = 0, 1, 2)$ refer to the Dirichlet and Neumann boundary conditions for $\boldsymbol{u}$ of different partial derivative

orders; $\partial\Omega_D^0$ designates the constraints of the displacement, $\partial\Omega_D^1$ denotes the constraints of the displacement gradient (e.g. fixed rotation state) and $\partial\Omega_D^1$ describes the displacement second-gradient; $\bar{\boldsymbol{P}}$ is the traction load, $\bar{\boldsymbol{Q}}$ refers to the couple stress load and $\bar{\boldsymbol{R}}$ is the higher order couple stress load.

Gradient elasticity deals not only with the gradient of the deformation but also the gradient of inertia terms [3, 25, 27, 28]. The kinetic energy with velocity gradient can be written as [28]

$$\mathcal{K} = \int_{t_0}^{t_1} \int_{\Omega} \frac{1}{2}\rho\dot{\boldsymbol{u}} \cdot \dot{\boldsymbol{u}} + \frac{1}{2}\rho l_d^2 \nabla\dot{\boldsymbol{u}} : \nabla\dot{\boldsymbol{u}} \tag{41}$$

The variation of the kinetic energy can be written as

$$\begin{aligned}
\delta\mathcal{K} &= \int_{t_0}^{t_1} \int_{\Omega} \rho\dot{\boldsymbol{u}} \cdot \delta\dot{\boldsymbol{u}} + \rho l_d^2 \nabla\dot{\boldsymbol{u}} : \nabla\delta\dot{\boldsymbol{u}} \\
&= \int_{t_0}^{t_1} \int_{\Omega} -\rho\ddot{\boldsymbol{u}} \cdot \delta\boldsymbol{u} - \rho l_d^2 \nabla\ddot{\boldsymbol{u}} : \nabla\delta\boldsymbol{u} \\
&= \int_{t_0}^{t_1} \int_{\Omega} -\rho\ddot{\boldsymbol{u}} \cdot \delta\boldsymbol{u} + \rho l_d^2 \nabla \cdot \nabla\ddot{\boldsymbol{u}} \cdot \delta\boldsymbol{u}
\end{aligned} \tag{42}$$

For any $\delta\boldsymbol{u}, \delta\nabla_n\boldsymbol{u}, \delta\nabla_n\nabla\boldsymbol{u}$, the Hamilton principle

$$\delta\mathcal{K} - \int_{t_0}^{t_1} \delta\mathcal{F}_{int} + \int_{t_0}^{t_1} \delta\mathcal{F}_{ext} = 0 \tag{43}$$

leads to

$$\rho\ddot{\boldsymbol{u}} - l_d^2 \nabla \cdot \nabla\ddot{\boldsymbol{u}} = -\boldsymbol{b} + \nabla \cdot (\boldsymbol{S}_1 - \nabla \cdot (\boldsymbol{S}_2 - \nabla \cdot \boldsymbol{S}_3)) \text{ in } \Omega \tag{44a}$$

$$\boldsymbol{u} = \bar{\boldsymbol{u}} \text{ on } \partial\Omega_D^0 \tag{44b}$$

$$\boldsymbol{P} = \bar{\boldsymbol{P}} \text{ on } \partial\Omega_N^0 \tag{44c}$$

$$\nabla_n\boldsymbol{u} = \overline{\nabla_n\boldsymbol{u}} \text{ on } \partial\Omega_D^1 \tag{44d}$$

$$\boldsymbol{Q} = \bar{\boldsymbol{Q}} \text{ on } \partial\Omega_N^1 \tag{44e}$$

$$\nabla_n\nabla\boldsymbol{u} = \overline{\nabla_n\nabla\boldsymbol{u}} \text{ on } \partial\Omega_D^2 \tag{44f}$$

$$\boldsymbol{R} = \bar{\boldsymbol{R}} \text{ on } \partial\Omega_N^2 \tag{44g}$$

The derivation of energies based on variational principle leads very naturally to the governing equations and various boundary conditions. The maximal order of derivatives in Eq.44a and

$\boldsymbol{V}_2$ is 6, 5, respectively. Similarly, the variation of the strain energy density of strain gradient elasticity (E^1 elasticity) can be derived. By setting $\boldsymbol{S}_3 = 0$ in Eq.44 , we obtain the governing equations and boundary conditions of gradient elasticity

$$\rho\ddot{\boldsymbol{u}} - l_d^2 \nabla \cdot \nabla \ddot{\boldsymbol{u}} = -\boldsymbol{b} + \nabla \cdot (\boldsymbol{S}_1 - \nabla \cdot \boldsymbol{S}_2) \text{ in } \Omega \tag{45a}$$

$$\boldsymbol{u} = \bar{\boldsymbol{u}} \text{ on } \partial\Omega_D^0 \tag{45b}$$

$$\boldsymbol{P} = \bar{\boldsymbol{P}} \text{ on } \partial\Omega_N^0 \tag{45c}$$

$$\nabla_n \boldsymbol{u} = \overline{\nabla_n \boldsymbol{u}} \text{ on } \partial\Omega_D^1 \tag{45d}$$

$$\boldsymbol{Q} = \bar{\boldsymbol{Q}} \text{ on } \partial\Omega_N^1 \tag{45e}$$

where $\boldsymbol{Q} = \boldsymbol{n} \cdot \boldsymbol{S}_2, \boldsymbol{P} = (g\boldsymbol{n} \cdot (\boldsymbol{n} \cdot \boldsymbol{S}_2) - \nabla_t \cdot (\boldsymbol{n} \cdot \boldsymbol{S}_2) + \boldsymbol{n} \cdot (\boldsymbol{S}_1 - \nabla \cdot \boldsymbol{S}_2))$, $\partial\Omega_D^i, \partial\Omega_N^i, (i = 0, 1)$ indicate the Dirichlet and Neumann boundary conditions for $\boldsymbol{u}$ of different partial derivative orders.

4. Numerical implementation

4.1. Review of Nonlocal Operator Method

NOM uses the integral form to replace the partial differential derivatives of different orders. We adopted a Total Lagrangian description of motion for the higher order gradient elasticity NOM. Consider a domain as shown in Fig.2(a), let $\boldsymbol{X}_i$ be spatial coordinates in the domain $\boldsymbol{\Omega}$; $\boldsymbol{r} := \boldsymbol{X}_j - \boldsymbol{X}_i$ is a spatial vector ranging from $\boldsymbol{X}_i$ to $\boldsymbol{X}_j$; $\boldsymbol{v}_i := \boldsymbol{v}(\boldsymbol{X}_i, t)$ and $\boldsymbol{v}_j := \boldsymbol{v}(\boldsymbol{X}_j, t)$ are the field values for $\boldsymbol{X}_i$ and $\boldsymbol{X}_j$, respectively; $\boldsymbol{v}_{ij} := \boldsymbol{v}_j - \boldsymbol{v}_i$ is the relative field vector for spatial vector $\boldsymbol{r}$.

Support $\mathcal{S}_i$ of point $\boldsymbol{X}_i$ is the neighborhood of point $\boldsymbol{X}_i$. A point $\boldsymbol{X}_j$ in support $\mathcal{S}_i$ forms the spatial vector $\boldsymbol{r}(= \boldsymbol{X}_j - \boldsymbol{X}_i)$. The support in the NOM can be a spherical domain, a cube, semi-spherical domain and so on.

Dual-support is defined as a union of points whose supports include $\boldsymbol{X}$, denoted by

$$\mathcal{S}_i' = \{\boldsymbol{X}_j | \boldsymbol{X}_i \in \mathcal{S}_j\}. \tag{46}$$

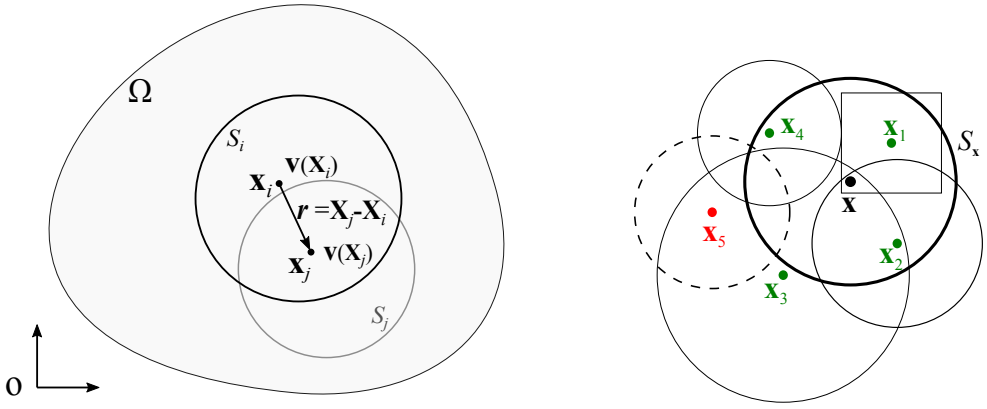

(a) (b)

Figure 2: (a) Domain and notation. (b) Schematic diagram for support and dual-support, all shapes above are supports, $\mathcal{S}_{\boldsymbol{X}} = \{\boldsymbol{X}_1, \boldsymbol{X}_2, \boldsymbol{X}_4\}$, $\mathcal{S}'_{\boldsymbol{X}} = \{\boldsymbol{X}_1, \boldsymbol{X}_2, \boldsymbol{X}_3\}$.

Point $\boldsymbol{X}_j$ forms the dual-vector $\boldsymbol{r}'(= \boldsymbol{X}_i - \boldsymbol{X}_j = -\boldsymbol{r})$ in $\mathcal{S}'_i$. On the other hand, $\boldsymbol{r}'$ is the spatial vector formed in $\mathcal{S}_j$. One example to illustrate the support and dual-support is shown in Fig.2(b).

The first-order nonlocal operator method uses the basic nonlocal operators to replace the local operator in calculus such as the gradient, divergence and curl operators. The functional formulated by the local differential operator can be used to construct the residual or tangent stiffness matrix by replacing the local operator with the corresponding nonlocal operator. The nonlocal gradient of a vector field $\boldsymbol{v}$ for point $\boldsymbol{X}_i$ in support $\mathcal{S}_i$ is defined as

$$\tilde{\nabla}\boldsymbol{v}_i := \int_{\mathcal{S}_i} w(\boldsymbol{r})\boldsymbol{v}_{ij} \otimes \boldsymbol{r}\ \mathrm{d}V_j \cdot \Big(\int_{\mathcal{S}_i} w(\boldsymbol{r})\boldsymbol{r} \otimes \boldsymbol{r}\ \mathrm{d}V_j\Big)^{-1}. \tag{47}$$

The nonlocal gradient operator and its variation in discrete form are given by

$$\tilde{\nabla}\boldsymbol{v}_i = \sum_{j\in\mathcal{S}_i} w(\boldsymbol{r})\boldsymbol{v}_{ij} \otimes \boldsymbol{r}\Delta V_j \cdot \Big(\sum_{j\in\mathcal{S}_i} w(\boldsymbol{r})\boldsymbol{r} \otimes \boldsymbol{r}\Delta V_j\Big)^{-1}, \tag{48}$$

$$\tilde{\nabla}\delta\boldsymbol{v}_i = \sum_{j\in\mathcal{S}_i} w(\boldsymbol{r})\delta\boldsymbol{v}_{ij} \otimes \boldsymbol{r}\Delta V_j \cdot \Big(\sum_{j\in\mathcal{S}_i} w(\boldsymbol{r})\boldsymbol{r} \otimes \boldsymbol{r}\Delta V_j\Big)^{-1}. \tag{49}$$

The operator energy functional for a vector field at point $\boldsymbol{x}_i$ is

$$\mathcal{F}_i^{hg} = p^{hg} \int_{\mathcal{S}_i} w(\boldsymbol{r})(\tilde{\nabla}\boldsymbol{v}_i \cdot \boldsymbol{r} - \boldsymbol{v}_{ij}) \cdot (\tilde{\nabla}\boldsymbol{v}_i \cdot \boldsymbol{r} - \boldsymbol{v}_{ij})\ \mathbf{d}V_j \tag{50}$$

where p^{hg} is a penalty coefficient. The residual and tangent stiffness matrix of $\mathcal{F}_i^{hg}$ can be obtained with ease, see [47] for more details. For problems that require higher order continuity, the higher order NOM is needed. According to Ref [46], a scalar field u_j at a point $j \in \mathcal{S}_i$ can be obtained by a Taylor series expansion at u_i in d dimensions with maximal derivative order not higher than n,

$$u_j = u_i + \sum_{(n_1,...,n_d)\in\alpha_d^n} \frac{r_1^{n_1}...r_d^{n_d}}{n_1!...n_d!} u_{i,n_1...n_d} + O(r^{|\alpha|+1}) \tag{51}$$

with

$$\boldsymbol{r} = (r_1, ..., r_d) = (X_{j1} - X_{i1}, ..., X_{jd} - X_{id}) \tag{52a}$$

$$u_{i,n_1...n_d} = \frac{\partial^{n_1+...+n_d} u_i}{\partial X_{i1}^{n_1}...\partial X_{id}^{n_d}} \tag{52b}$$

$$|\alpha| = \max\left(n_1 + ... + n_d\right) \tag{52c}$$

α_d^n being the list of multi-indexes, given by

$$\alpha_d^n = \{(n_1, ..., n_d) | 1 \le \sum_{i=1}^{d} n_i \le n,\ n_i \in \mathbb{N}^0, 1 \le i \le d\} \tag{53}$$

and $\mathbb{N}^0 = \{0, 1, 2, 3, ...\}$. The number of multi-indices in α_d^n is $(n+d)!/(n!d!) - 1$ and all elements in α_d^n of Eq.53 can be obtained easily by Mathematica [46]. For any multi-index $(n_1, ..., n_d) \in \alpha_d^n$, the partial derivative and the polynomial are

$$u_{i,n_1...n_d},\ \frac{r_1^{n_1}...r_d^{n_d}}{n_1!...n_d!}, \quad \forall (n_1, ..., n_d) \in \alpha_d^n. \tag{54}$$

When the length scale of support $\mathcal{S}_i$ at u_i is taken into account, the Taylor series expansion in Eq.51 can be written as

$$\begin{aligned} u_j &= u_i + \sum_{(n_1,...,n_d)\in\alpha_d^n} \frac{r_1^{n_1}...r_d^{n_d}}{h_i^{n_1+...+n_d}} \Big(\frac{h_i^{n_1+...+n_d}}{n_1!...n_d!} u_{i,n_1...n_d} \Big) + O(r^{n+1}) \\ &= u_i + \sum_{(n_1,...,n_d)\in\alpha_d^n} \frac{r_1^{n_1}...r_d^{n_d}}{h_i^{n_1+...+n_d}}\ u_{i,n_1...n_d}^h + O(r^{n+1}) \end{aligned} \tag{55}$$

where h_i is the characteristic length of $\mathcal{S}_i$, and

$$u^h_{i,n_1...n_d} = \frac{h_i^{n_1+...+n_d}}{n_1!...n_d!} u_{i,n_1...n_d} \tag{56}$$

Let $\boldsymbol{p}^h_j$, $\partial^h_\alpha u_i$ and $\partial_\alpha u_i$ denote the list of the polynomials, scaled partial derivatives, partial derivatives, respectively, based on multi-index notation α^n_d in Eq.53,

$$\boldsymbol{p}^h_j = (\frac{r_d}{h}, ..., \frac{r_1^{n_1}...r_d^{n_d}}{h^{n_1+...+n_d}}, ..., \frac{r_1^n}{h^n})^T \tag{57a}$$

$$\partial^h_\alpha u_i = (u^h_{i,0...1}, ..., u^h_{i,n_1...n_d}, ..., u^h_{i,n...0})^T \tag{57b}$$

$$\partial_\alpha u_i = (u_{i,0...1}, ..., u_{i,n_1...n_d}, ..., u_{i,n...0})^T. \tag{57c}$$

$\partial^h_\alpha u_i$ and $\partial_\alpha u_i$ are related by

$$\partial_\alpha u_i = \boldsymbol{H}_i^{-1} \partial^h_\alpha u_i, \text{ with } \boldsymbol{H}_i = \text{diag}\big[h_i, ..., \frac{h_i^{n_1+...+n_d}}{n_1!...n_d!}, ..., \frac{h_i^n}{n!}\big] \tag{58}$$

where $\text{diag}[a_1, ..., a_n]$ denotes a diagonal matrix whose diagonal entries starting in the upper left corner are $a_1, ..., a_n$. Therefore, the Taylor series expansion with u_i being moved to the left side of the equation can be written as

$$u_{ij} = (\partial^h_\alpha u_i)^T \boldsymbol{p}^h_j, \forall j \in \mathcal{S}_i \tag{59}$$

where $u_{ij} = u_j - u_i$. Integrating u_{ij} with weighted coefficient $w(\boldsymbol{r})(\boldsymbol{p}^h_j)^T$ in support $\mathcal{S}_i$, we obtain

$$\begin{aligned}\int_{\mathcal{S}_i} w(\boldsymbol{r}) u_{ij} (\boldsymbol{p}^h_j)^T \, \mathrm{d}V_j &= (\partial^h_\alpha u_i)^T \int_{\mathcal{S}_i} w(\boldsymbol{r}) \boldsymbol{p}^h_j \otimes (\boldsymbol{p}^h_j)^T \, \mathrm{d}V_j \\ &= (\partial_\alpha u_i)^T \boldsymbol{H}_i \int_{\mathcal{S}_i} w(\boldsymbol{r}) \boldsymbol{p}^h_j \otimes (\boldsymbol{p}^h_j)^T \, \mathrm{d}V_j \end{aligned} \tag{60}$$

where $w(\boldsymbol{r})$ is the weight function. Thus, the nonlocal operator $\tilde{\partial}_\alpha u_i$ can be obtained as

$$\tilde{\partial}_\alpha u_i := \boldsymbol{H}_i^{-1} \Big(\int_{\mathcal{S}_i} w(\boldsymbol{r}) \boldsymbol{p}^h_j \otimes (\boldsymbol{p}^h_j)^T \, \mathrm{d}V_j \Big)^{-1} \int_{\mathcal{S}_i} w(\boldsymbol{r}) u_{ij} \boldsymbol{p}^h_j \, \mathrm{d}V_j = \boldsymbol{K}_i \cdot \int_{\mathcal{S}_i} w(\boldsymbol{r}) \boldsymbol{p}^h_j u_{ij} \, \mathrm{d}V_j \tag{61}$$

with

$$\boldsymbol{K}_i := \boldsymbol{H}_i^{-1} \Big(\int_{\mathcal{S}_i} w(\boldsymbol{r}) \boldsymbol{p}^h_j \otimes (\boldsymbol{p}^h_j)^T \, \mathrm{d}V_j \Big)^{-1}. \tag{62}$$

The variation of $\tilde{\partial}_\alpha u_i$ is

$$\tilde{\partial}_\alpha \delta u_i := \boldsymbol{K}_i \cdot \int_{\mathcal{S}_i} w(\boldsymbol{r}) \boldsymbol{p}_j^h (\delta u_j - \delta u_i) \, \mathrm{d}V_j \tag{63}$$

In the continuous form, the number of dimensions of $\partial \delta u_i$ is infinite and a discretization is required. After discretization of the domain by particles, the whole domain is represented by

$$\Omega = \sum_{i=1}^{N} \Delta V_i \tag{64}$$

where i is the global index of volume ΔV_i and N is the number of particles in Ω. Particles in $\mathcal{S}_i$ are represented by

$$\mathcal{S}_i = \{j_1, ..., j_k, ..., j_{n_i}\} \tag{65}$$

where $j_1, ..., j_k, ..., j_{n_i}$ are the global indices of neighboring particle i and n_i is the number of neighbors of i in $\mathcal{S}_i$. The discrete form of Eq.61 and its variation are

$$\tilde{\partial}_\alpha u_i = \boldsymbol{K}_i \cdot \sum_{j \in \mathcal{S}_i} u_{ij} w(\boldsymbol{r}_j) \boldsymbol{p}_j^h \Delta V_j = \boldsymbol{K}_i \boldsymbol{p}_{wi}^h \Delta \boldsymbol{u}_i \tag{66a}$$

$$\tilde{\partial}_\alpha \delta u_i = \boldsymbol{K}_i \cdot \sum_{j \in \mathcal{S}_i} \delta u_{ij} w(\boldsymbol{r}_j) \boldsymbol{p}_j^h \Delta V_j = \boldsymbol{K}_i \boldsymbol{p}_{wi}^h \delta \Delta \boldsymbol{u}_i \tag{66b}$$

with

$$\boldsymbol{K}_i = \boldsymbol{H}_i^{-1} \Big(\sum_{j \in \mathcal{S}_i} w(\boldsymbol{r}) \boldsymbol{p}_j^h \otimes (\boldsymbol{p}_j^h)^T \Delta V_j \Big)^{-1}, \tag{67a}$$

$$\boldsymbol{p}_{wi}^h = \Big(w(\boldsymbol{r}_{j_1}) \boldsymbol{p}_{j_1}^h \Delta V_{j_1}, ..., w(\boldsymbol{r}_{j_{n_i}}) \boldsymbol{p}_{j_{n_i}}^h \Delta V_{j_{n_i}} \Big) \tag{67b}$$

$$\Delta \boldsymbol{u}_i = (u_{ij_1}, ..., u_{ij_k}, ..., u_{ij_{n_i}})^T \tag{67c}$$

The nonlocal operator provides all partial derivatives with maximal order for a single index up to n. The set of derivatives in PDEs of real application is a subset of the nonlocal operator. Together with the weak formulation (weighted residual method or variational principles (i.e.[47])), Eq.66a can be employed to solve many linear (nonlinear) PDEs. Eq.66a can be written more concisely as

$$\tilde{\partial}_\alpha u_i = \boldsymbol{K}_i \boldsymbol{p}_{wi}^h \Delta \boldsymbol{u}_i = \boldsymbol{B}_{\alpha i} \boldsymbol{u}_i \tag{68}$$

with $\boldsymbol{B}_{\alpha i}$ being the operator matrix for point i based on multi-index α_d^n

$$\boldsymbol{B}_{\alpha i} = \begin{bmatrix} -(1,\cdots,1)_{n_p}\boldsymbol{K}_i\boldsymbol{p}_{wi}^h \\ \boldsymbol{K}_i\boldsymbol{p}_{wi}^h \end{bmatrix} \tag{69}$$

$$\boldsymbol{u}_i = (u_i, u_{j_1}, u_{j_2}, \cdots, u_{j_{n_i}})^T \tag{70}$$

where $(1,\cdots,1)_{n_p}\boldsymbol{K}_i\boldsymbol{p}_{wi}^h$ is the column sum of $\boldsymbol{K}_i\boldsymbol{p}_{wi}^h$, n_p is the length of α_d^n. The operator matrix obtains all partial derivatives of maximal order less than $|\alpha|+1$ by the nodal values in the support. For real applications, one can select the specific rows in the operator matrix based on the partial derivatives contained in the specific PDEs. For example, if the order of derivatives in the given PDEs are $\tilde{\partial} u_i = (u_{i,Y}, u_{i,YY}, u_{i,XY})^T \subset \tilde{\partial}_\alpha u_i$, one can select the blue lines in Eq.71 to form the actually operator matrix given by $\boldsymbol{B}_i$ in Eq.72.

$$\underbrace{\begin{bmatrix} u_{i,Y} \\ u_{i,X} \\ u_{i,YY} \\ u_{i,XY} \\ u_{i,XX} \\ \vdots \end{bmatrix}}_{\tilde{\partial}_\alpha u_i} = \underbrace{\begin{bmatrix} b_{11} & b_{12} & \cdots & b_{1(n+1)} \\ b_{21} & b_{22} & \cdots & b_{2(n+1)} \\ b_{31} & b_{32} & \cdots & b_{3(n+1)} \\ b_{41} & b_{42} & \cdots & b_{4(n+1)} \\ \vdots & \vdots & \ddots & \vdots \\ b_{m1} & b_{m2} & \cdots & b_{m(n+1)} \end{bmatrix}}_{\boldsymbol{B_{\alpha i}}} \underbrace{\begin{bmatrix} u_i \\ u_{j_1} \\ \vdots \\ u_{j_n} \end{bmatrix}}_{\boldsymbol{u}_i} \tag{71}$$

$$\underbrace{\begin{bmatrix} u_{i,Y} \\ u_{i,YY} \\ u_{i,XY} \end{bmatrix}}_{\tilde{\partial} u_i} = \underbrace{\begin{bmatrix} b_{11} & b_{12} & \cdots & b_{1(n+1)} \\ b_{31} & b_{32} & \cdots & b_{3(n+1)} \\ b_{41} & b_{42} & \cdots & b_{4(n+1)} \end{bmatrix}}_{\boldsymbol{B_i}} \underbrace{\begin{bmatrix} u_i \\ u_{j_1} \\ \vdots \\ u_{j_n} \end{bmatrix}}_{\boldsymbol{u}_i} \tag{72}$$

For a given maximal differential order and number of space dimensions, NOM offers the derivatives of all orders in discrete form 'automatically'. These nonlocal derivatives are similar to the derivatives of the shape functions in IGA. When the selected derivatives are

inserted into the equivalent functional of the physical problem in discrete form, the residual and tangent stiffness matrix of the functional can be derived.

Besides considering the functional for the physical problem, the functional for the nonlocal operators should be considered explicitly. The energy functional for all nonlocal operators is defined as [46]

$$\mathcal{F}_i(\boldsymbol{u}) = \sum_{j\in\mathcal{S}_i} w(\boldsymbol{r})\big(u_{ij} - (\boldsymbol{p}_j^h)^T\tilde{\partial}_\alpha^h u_i\big)^2\Delta V_j \tag{73}$$

Based on Eq.66a, $\mathcal{F}_i(\boldsymbol{u})$ can be simplified as

$$\begin{aligned}\mathcal{F}_i(\boldsymbol{u}) =& \sum_{j\in\mathcal{S}_i} w(\boldsymbol{r})u_{ij}^2\Delta V_j - \Delta\boldsymbol{u}_i^T(\boldsymbol{p}_{wi}^h)^T\Big(\sum_{j\in\mathcal{S}_i} w(\boldsymbol{r})\boldsymbol{p}_j^h(\boldsymbol{p}_j^h)^T\Delta V_j\Big)^{-1}\boldsymbol{p}_{wi}^h\Delta\boldsymbol{u}_i\\ =&\Delta\boldsymbol{u}_i^T\Big(\mathrm{diag}\big[w(\boldsymbol{r}_{j_1})\Delta V_{j_1},...,w(\boldsymbol{r}_{j_{n_i}})\Delta V_{j_{n_i}}\big] - (\boldsymbol{p}_{wi}^h)^T\Big(\sum_{j\in\mathcal{S}_i} w(\boldsymbol{r})\boldsymbol{p}_j^h(\boldsymbol{p}_j^h)^T\Delta V_j\Big)^{-1}\boldsymbol{p}_{wi}^h\Big)\Delta\boldsymbol{u}_i\\ =&\Delta\boldsymbol{u}_i^T\boldsymbol{M}_i\Delta\boldsymbol{u}_i\end{aligned} \tag{74}$$

with

$$\boldsymbol{M}_i = \mathrm{diag}\big[w(\boldsymbol{r}_{j_1})\Delta V_{j_1},...,w(\boldsymbol{r}_{j_{n_i}})\Delta V_{j_{n_i}}\big] - (\boldsymbol{p}_{wi}^h)^T\Big(\sum_{j\in\mathcal{S}_i} w(\boldsymbol{r})\boldsymbol{p}_j^h(\boldsymbol{p}_j^h)^T\Delta V_j\Big)^{-1}\boldsymbol{p}_{wi}^h \tag{75}$$

Apparently, $\boldsymbol{M}_i$ is a symmetric matrix. The expression of $\mathcal{F}_i(\boldsymbol{u})$ is quadratic, and its Hessian matrix can be extracted as

$$\boldsymbol{K}_i^{hg} = \frac{p_{hg}}{m_i}\begin{bmatrix}\sum\boldsymbol{v}_i & -\boldsymbol{v}_i^T\\ -\boldsymbol{v}_i & \boldsymbol{M}_i\end{bmatrix} \tag{76}$$

where $\boldsymbol{v}_i(j) = \sum_{k=1}^{n_i}\boldsymbol{M}_i(j,k)$ is the sum of the row of $\boldsymbol{M}_i$; the first row (column) denotes the entries for point i, while the neighbors start from the second row (column), p_{hg} is a penalty coefficient and m_i the normalization coefficient given by $m_i = \sum_{j\in\mathcal{S}_i} w(\boldsymbol{r})\boldsymbol{r}\cdot\boldsymbol{r}\Delta V_j$. The reader is referred to [46] for more details of the NOM.

4.2. Newton-Raphson method

The governing equations and boundary conditions in Eq.44 are quite complicated. The highest continuity in $\boldsymbol{Q}$ is C^4 and the gradient and Hessian matrix of the functional on

boundary $\partial\Omega_D^1$ are cumbersome. Note that NOM does not satisfy the Kronecker-Delta property, and the order of NOM should be at least C^5 in order to satisfy the Dirichlet boundary conditions on $\partial\Omega_D^0$, where the continuity order in $\boldsymbol{P}$ is C^5. Therefore, we employ the penalty method to enforce both Dirichlet boundary conditions and the normal Dirichlet boundary conditions. The equivalent energy functional of second-gradient elasticity then becomes

$$\begin{aligned}\mathcal{F} = &\int_\Omega \phi(\boldsymbol{u}, \nabla\boldsymbol{u}, \nabla^2\boldsymbol{u}, \nabla^3\boldsymbol{u})\ \mathrm{d}V + \int_{\partial\Omega_D^0} \alpha_1(\boldsymbol{u}-\bar{\boldsymbol{u}})\cdot(\boldsymbol{u}-\bar{\boldsymbol{u}})\ \mathrm{d}S - \int_{\partial\Omega_N^0} \bar{\boldsymbol{P}}\cdot\boldsymbol{u}\ \mathrm{d}S \\ &+ \int_{\partial\Omega_D^1} \alpha_2(\nabla_n\boldsymbol{u} - \overline{\nabla_n\boldsymbol{u}}) : (\nabla_n\boldsymbol{u} - \overline{\nabla_n\boldsymbol{u}})\ \mathrm{d}S - \int_{\partial\Omega_N^1} \bar{\boldsymbol{Q}} : \nabla_n\boldsymbol{u}\ \mathrm{d}S \end{aligned} \tag{77}$$

where α_1, α_2 are penalty parameters. One advantage of the penalty method is that the highest order of partial derivatives is 4 for third-gradient elasticity, while the formulation based on the modified variational principle requires C^7 continuity. We neglect the terms on $\partial\Omega_D^2$ and $\partial\Omega_N^2$ for simplicity.

After discretization, the discrete form of the functional in Eq.77 becomes

$$\begin{aligned}\mathcal{F} = &\sum_{\Delta V_i\in\Omega} \phi(\boldsymbol{u}_i, \nabla\boldsymbol{u}_i, \nabla^2\boldsymbol{u}_i, \nabla^3\boldsymbol{u}_i)\Delta V_i \\ &+ \sum_{\Delta S_i\in\partial\Omega_D^0} \alpha_1(\boldsymbol{u}_i-\bar{\boldsymbol{u}}_i)\cdot(\boldsymbol{u}_i-\bar{\boldsymbol{u}}_i)\Delta S_i - \sum_{\Delta S_i\in\partial\Omega_N^0} \bar{\boldsymbol{P}}_i\cdot\boldsymbol{u}_i\Delta S_i \\ &+ \sum_{\Delta S_i\in\partial\Omega_D^1} \alpha_2(\nabla_n\boldsymbol{u}_i - \overline{\nabla_n\boldsymbol{u}_i}) : (\nabla_n\boldsymbol{u}_i - \overline{\nabla_n\boldsymbol{u}_i})\Delta S_i - \sum_{\Delta S_i\in\partial\Omega_N^1} \bar{\boldsymbol{Q}}_i : \nabla_n\boldsymbol{u}_i\Delta S_i \end{aligned} \tag{78}$$

The differential derivatives in ϕ of E^3 elasticity with unknowns $\boldsymbol{u} = (u, v)^T$ in material coordinates $\boldsymbol{X} = (X, Y)$ are

$$\begin{aligned}\partial\boldsymbol{U}_{2d} = \Big(&u_{,Y}, v_{,Y}, u_{,X}, v_{,X}, u_{,YY}, v_{,YY}, u_{,XY}, v_{,XY}, u_{,XX}, v_{,XX}, u_{,YYY}, v_{,YYY}, \\ &u_{,XYY}, v_{,XYY}, u_{,XXY}, v_{,XXY}, u_{,XXX}, v_{,XXX}, u_{,YYYY}, v_{,YYYY}, u_{,XYYY}, \\ &v_{,XYYY}, u_{,XXYY}, v_{,XXYY}, u_{,XXXY}, v_{,XXXY}, u_{,XXXX}, v_{,XXXX}\Big)^T \end{aligned} \tag{79}$$

The differential derivatives in $\mathcal{F}$ of E^3 elasticity with unknowns $\boldsymbol{u} = (u, v, w)^T$ in material

coordinates $\boldsymbol{X} = (X, Y, Z)$ are

$$\partial \boldsymbol{U}_{3d} = \Big(\underbrace{u_{,Z}, v_{,Z}, w_{,Z}, ..., v_{,XY}, ..., u_{,XYZ}, ..., w_{,XXXX}}_{102\ terms} \Big)^T \tag{80}$$

In NOM, the differential derivatives can be written as $\partial \boldsymbol{U}_s = \boldsymbol{B}_s \boldsymbol{U}, s \in \{2d, 3d\}$, where $\boldsymbol{B}_s$ is the operator matrix constructed with steps similar to that in Eq.71 and $\boldsymbol{U}$ is the vector form of all unknowns in one support. In other words, for a given equivalent energy functional, the independent derivatives of various orders can be extracted, which form a subset of the list of nonlocal derivatives provided by NOM. The operator matrix $\boldsymbol{B}_s$ is formed by selecting a row with the same index of derivative in $\tilde{\partial}_\alpha u_i$. The residual vector and tangent stiffness matrix for one particle can be obtained as

$$\boldsymbol{R}_i = \frac{\partial \phi_i}{\partial \boldsymbol{U}} = \frac{\partial (\partial \boldsymbol{U})}{\partial \boldsymbol{U}} \frac{\partial \phi_i}{\partial (\partial \boldsymbol{U})} = \boldsymbol{B}^T \frac{\partial \phi_i}{\partial (\partial \boldsymbol{U})} \tag{81}$$

$$\boldsymbol{K}_i = \frac{\partial \boldsymbol{R}_i}{\partial \boldsymbol{U}} = \boldsymbol{B}^T \frac{\partial^2 \phi_i}{\partial (\partial \boldsymbol{U})^2} \boldsymbol{B} \tag{82}$$

The explicit forms of $\frac{\partial \phi}{\partial (\partial \boldsymbol{U})}$ and $\frac{\partial^2 \phi}{\partial (\partial \boldsymbol{U})^2}$ can be obtained by softwares such as Mathematica [57] allowing symbolic operations. For simplicity, we omit these lengthy expressions in the paper. However, the code will be made available. One can see that the construction of the residual vector and tangent stiffness matrix for each particle is a series of matrix multiplications. The global tangent stiffness matrix for the functional in domain Ω can be expressed as

$$\boldsymbol{R}_\Omega = \sum_{\Delta V_i \in \Omega} \boldsymbol{R}_i \Delta V_i, \qquad \boldsymbol{K}_\Omega = \sum_{\Delta V_i \in \Omega} \boldsymbol{K}_i \Delta V_i \tag{83}$$

The assembly of $\boldsymbol{R}_i, \boldsymbol{K}_i$ is based on the global indices of all unknowns in one support. The global tangent stiffness matrices (e.g. $\boldsymbol{K}_{\partial \Omega_D^0}, \boldsymbol{K}_{\partial \Omega_D^1}$) and residuals (e.g. $\boldsymbol{R}_{\partial \Omega_D^0}, \boldsymbol{R}_{\partial \Omega_D^1}$) for functionals on boundaries $\partial \Omega_D^0, \partial \Omega_D^1$ can be obtained in the same manner. The Neumann boundary condition on $\partial \Omega_N^0$ can be applied directly on the particles. The moment boundary condition on $\partial \Omega_N^1$ can be enforced by calculating the residual

$$\boldsymbol{R}_{\partial \Omega_N^1} = \sum_{\Delta S_i \in \partial \Omega_N^1} \frac{\partial \phi_N}{\partial (\partial \boldsymbol{U}_N)} \frac{\partial (\partial \boldsymbol{U}_N)}{\partial \boldsymbol{U}} \Delta S_i = \sum_{\Delta S_i \in \partial \Omega_N^1} \boldsymbol{B}_N^T \frac{\partial \phi_N}{\partial (\partial \boldsymbol{U})} \Delta S_i \tag{84}$$

where $\phi_N = \bar{\boldsymbol{Q}} : \nabla_n \boldsymbol{u}$ and $\partial \boldsymbol{U}_N = \nabla \otimes \boldsymbol{u} = \boldsymbol{B}_N \boldsymbol{U}$; $\boldsymbol{B}_N$ are constructed by selecting the first 2 rows or 3 rows of $\boldsymbol{B}$ in 2D or 3D, respectively; $\frac{\partial \phi_N}{\partial(\partial \boldsymbol{U}_N)}$ can be obtained by Mathematica [57]. Then, the global tangent stiffness matrix and residual are

$$\boldsymbol{R} = \boldsymbol{R}_\Omega + \boldsymbol{R}_{\partial\Omega_D^0} + \boldsymbol{R}_{\partial\Omega_D^1} + \boldsymbol{R}_{\partial\Omega_N^1} \tag{85}$$

$$\boldsymbol{K} = \boldsymbol{K}_\Omega + \boldsymbol{K}_{\partial\Omega_D^0} + \boldsymbol{K}_{\partial\Omega_D^1} \tag{86}$$

With the global residual and tangent stiffness available, a standard Newton Raphson method can be used to find the solution.

5. Numerical examples

In this section, we present several representative numerical examples to study the property of the E^n elasticity theory. The setup of the 2D/3D examples and the associated boundary conditions are outlined in Fig.3. The domain is discretized with a Cartesian grid. The particles in the void domain are removed to form holes. Each particle has the same number of neighbouring particles in the support, and the support size is selected as the distance between the furthest neighbour particle and the master particle in the support. So the central particles have a smaller support size compared to the particles close to the boundary. The number of neighbours in support is selected as $1/2(n^2 + 33n + 32)$ in 2D, where n is the order of gradient elasticity. The material parameters and length scales will be given in the subsections.

5.1. Convergence of strain energy in E^3 elasticity

The first example tests the strain energy distribution of E^3 elasticity for different discretizations. The material parameters are elastic modulus $E = 30$ GPa and Poisson's ratio $\nu = 0.3$. Plane stress conditions are assumed. The internal length scales are set to $l_1 = l_2 = l_3 = 0.05$. The geometry and boundary conditions are depicted in Fig.3(a). The left side of the plate is fixed in all directions and a uniform tension load of $p = 1$ GPa·m is applied on the right side, which results in a moderate deformation. Different discretizations such as $40^2, 60^2, 80^2, 96^2, 120^2, 160^2, 200^2$ particles are used to study the distribution

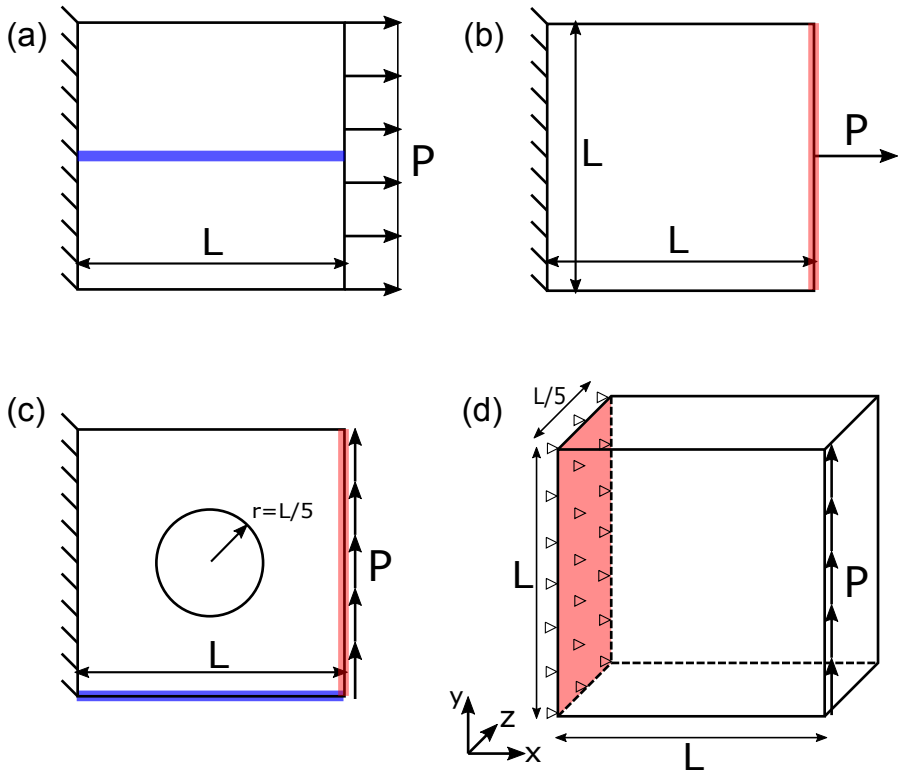

Figure 3: The setup of the 2D plate and 3D plate and boundary conditions.

of the strain energy of different orders. The engineering strain is approximately 0.0288 as depicted in Fig.4(a). The distribution of total strain energy density on each particle is given in Fig.4(b). The maximal strain energy density occurs around the corners. The total strain energies on different strain gradient orders can be found in Fig.5. With increasing the number of particles, the energies of different levels converge. The strain energy is dominant while the higher order energies tend to decrease with increasing gradient orders. Indeed, the deformation under pure tension load is "uniform" for this numerical example.

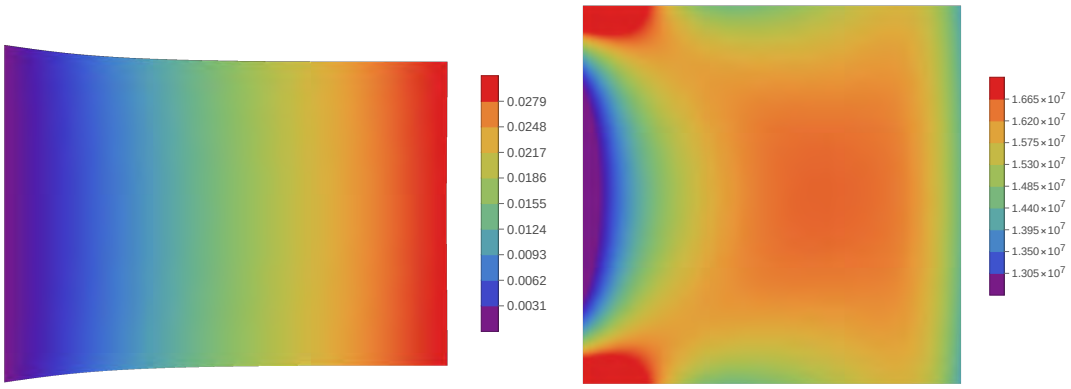

(a) (b)

Figure 4: (a) Deformation with unit of meters in x-direction, scaled by 10 times and (b) the distribution of total strain energy density with units of Joule per unit volume for discretization of 120^2 particles.

5.2. 2D plate with uniform deformation

The second example tests the influence of E^n gradient elasticity subjected to a uniform load; E^0, E^1, E^2 elasticity theories are implemented. The geometry and boundary conditions are illustrated in Fig.3(a). A plate with dimensions of $1 \times 1\, m^2$ is discretized into 81^2 particles. The material parameters are elastic modulus $E = 30$ GPa and Poisson's ratio $\nu = 0.3$. The internal length scales are $l_1 = l_2 = 0.05$. The left side of the plate is fixed in all directions and the right side is subjected to a uniform tension load of $p = 1$ MPa/m. Fig.6(a) shows that the displacement based on higher order elasticity theory is identical to conventional

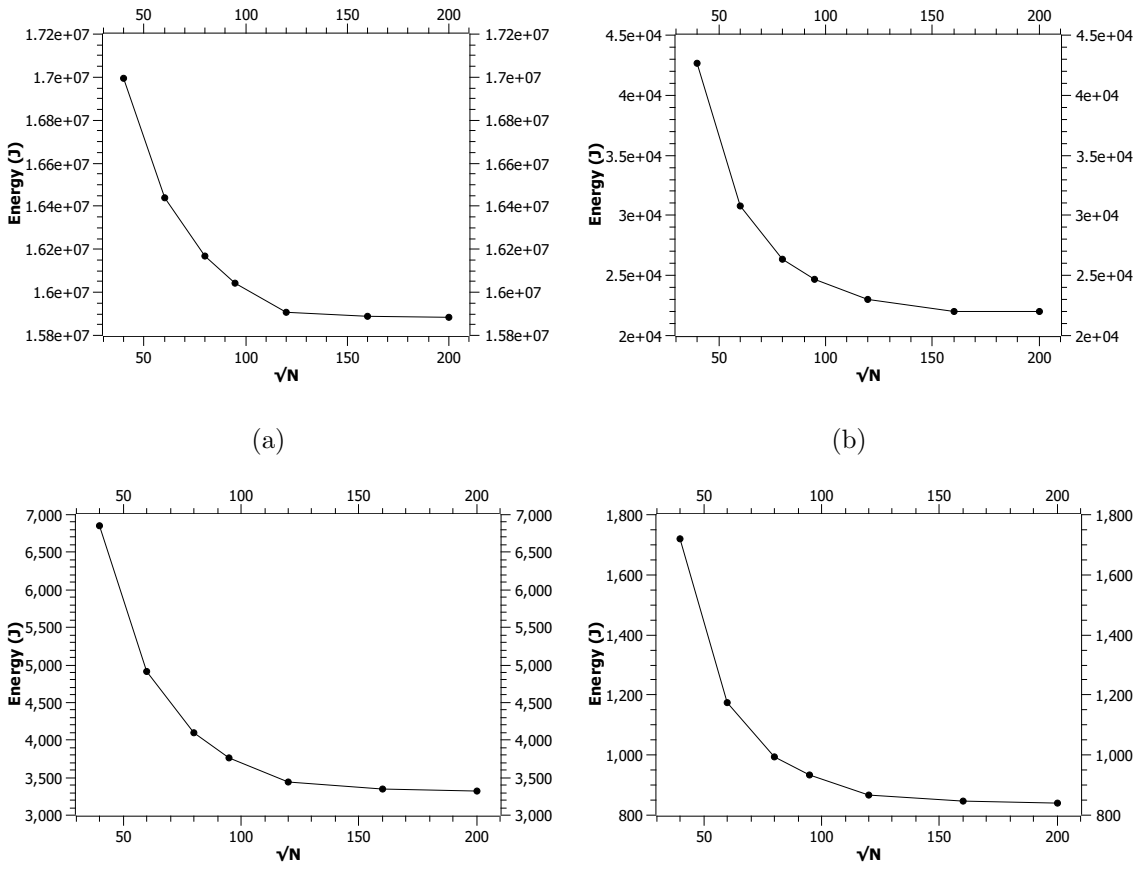

(a) (b)

(c) (d)

Figure 5: Total strain energy on level (a) $\frac{1}{2}\boldsymbol{S} : \boldsymbol{E}$; (b) $\frac{1}{2}l_1^2\nabla\boldsymbol{S}\vdots\nabla\boldsymbol{E}$; (c) $\frac{1}{2}l_2^4\nabla^2\boldsymbol{S} :: \nabla^2\boldsymbol{E}$ and (d) $\frac{1}{2}l_3^6\nabla^3\boldsymbol{S} \cdot^{(5)} \nabla^3\boldsymbol{E}$; N is the total number of particles.

elasticity for uniform deformations since the higher order strain components are quite small such that their contribution to the energy density can be neglected. However, the higher order terms make the deformation smoother as shown in Fig.6(b). This indicates that the higher order gradient elasticity should be tested with in-homogeneous deformations.

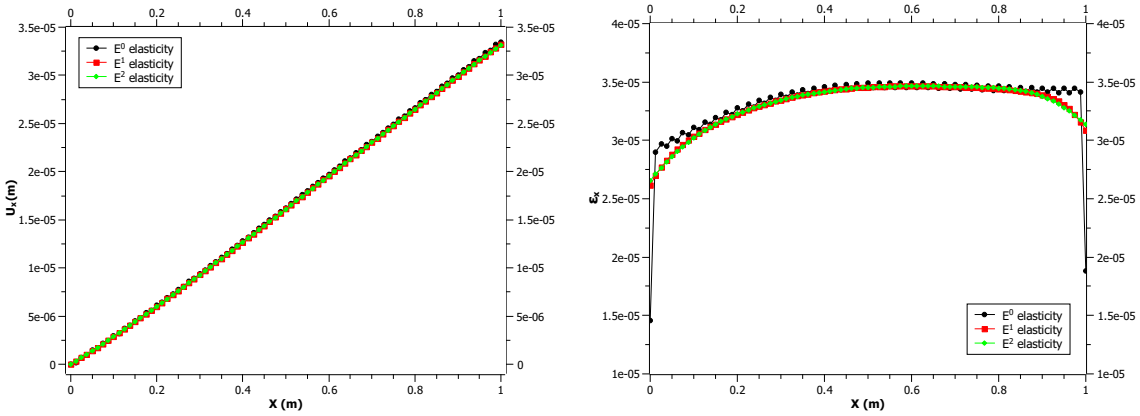

(a) (b)

Figure 6: (a) Displacement in x-direction and (b) strain in x-direction for particles on middle horizontal line (Blue line in Fig.3(a)).

5.3. 2D plate subjected to point force

Let us test the capability of gradient theory for point loads. We adopt the dimensions of the plate and its material parameters from the previous subsections. However, one particle in the middle of the right side boundary of the plate is subjected to a point force of 1000 N. The geometry and boundary conditions are depicted in Fig.3(b). The plate is discretized into 81x81 particles. $E^1 - E^4$ elasticity theories are considered. The deformations of the plate for E^1, E^2, E^3, E^4 elasticity can be found in Fig.7. Obviously, gradient elasticity can 'withstand' point loads. The higher order gradient elasticity has a smoother displacement field compared with gradient elasticity. This observation is consistent with the numerical analysis by FEM [16] and by IGA [58]. Comparisons of the displacement in x-direction of particles on the right side boundary (i.e.the red line in Fig.3(b)) are plotted in Fig.8. The first-order and second-order derivatives of the displacement in x-direction of particles are shown in Fig.9. The derivative of the displacement in E^1 elasticity changes sharply,

in contrast to the smooth transition of the displacement gradient in higher order gradient elasticity.

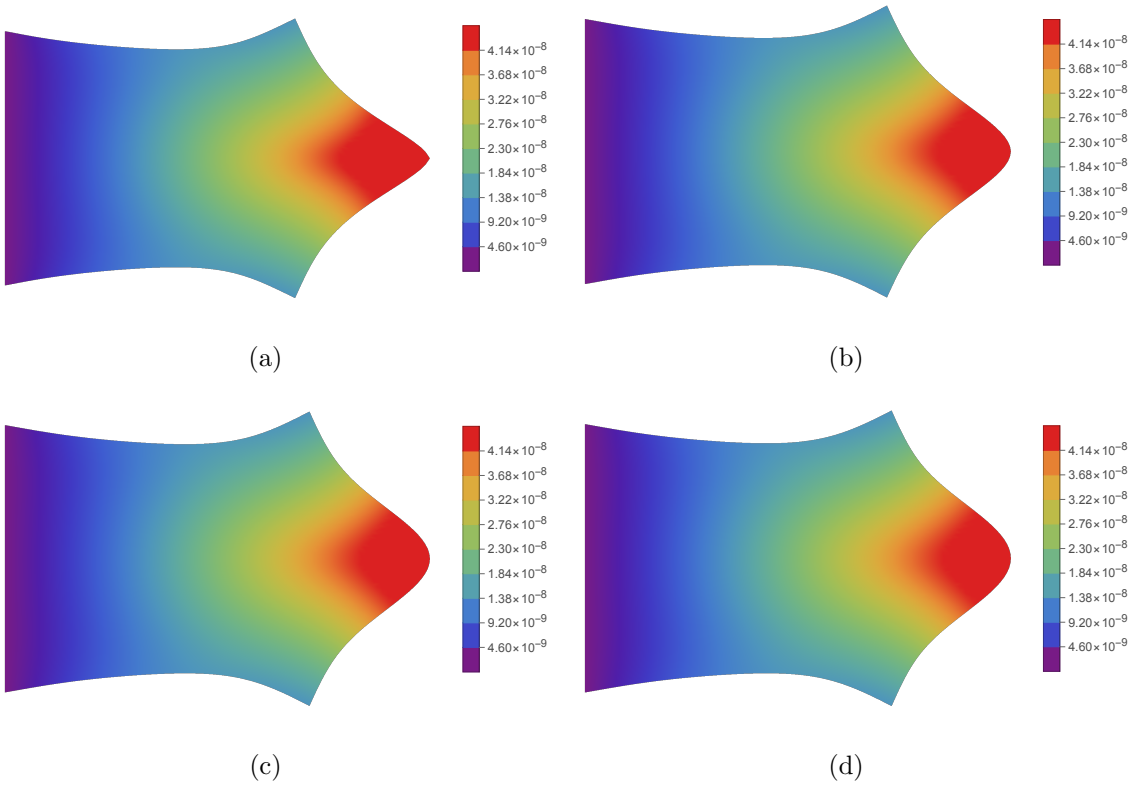

Figure 7: Displacement with unit of meters in x-direction of the plate with deformation scaled by 10^7 times for (a) E^1 elasticity, (b) E^2 elasticity, (c) E^3 elasticity and (d) E^4 elasticity.

5.4. Plate with a hole: influence of length scales

This example deals with a plate with a hole of radius 0.2 m located at the center. The geometry and boundary conditions are depicted in Fig.3(c). The same material parameters as before are used. The plate is discretized into 81x81 particles and then the particles falling inside the circle are removed. With different length scales, the displacement in x-direction of all particles on the right boundary of the plate based on (a) E^1 elasticity and (b) E^2 elasticity are shown in Fig.10. Higher length scale parameters can significantly reduce the stress concentration induced by the hole. The gradient of the displacement in x-direction of E^1 elasticity is shown in Fig.11, which means that a larger l_1 smoothes the strain field. The

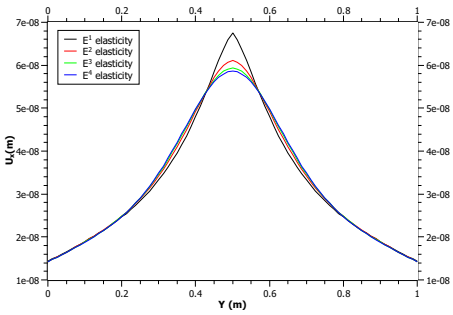

Figure 8: The deformation of all particles on the red line in Fig.3(b).

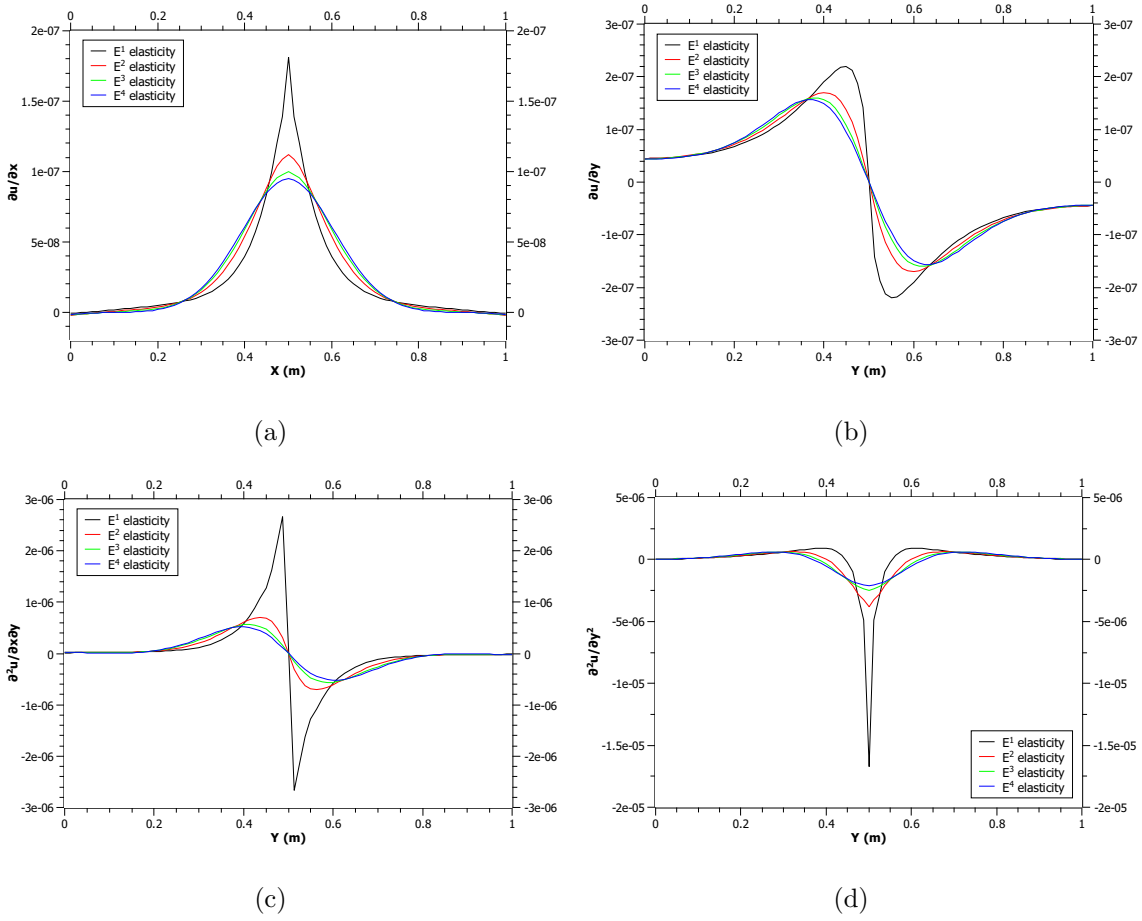

(a) (b)

(c) (d)

Figure 9: The first-order and second-order derivative of deformation of all particles on the red line in Fig.3(b).

displacement gradient in x-direction of E^2 elasticity can be found in Fig.12. The larger l_i, the smaller the strain field.

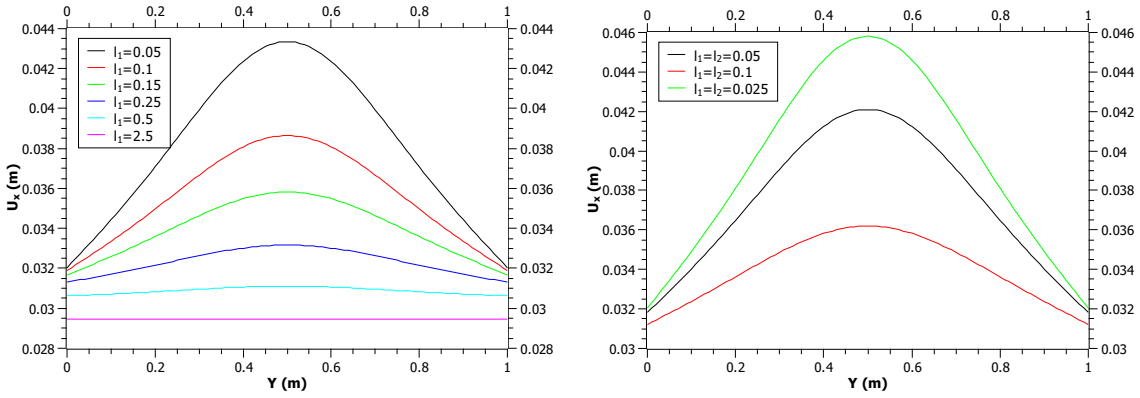

(a) (b)

Figure 10: The displacement in x-direction of particles on right side boundary of the plate based on (a) E^1 elasticity and (b) E^2 elasticity.

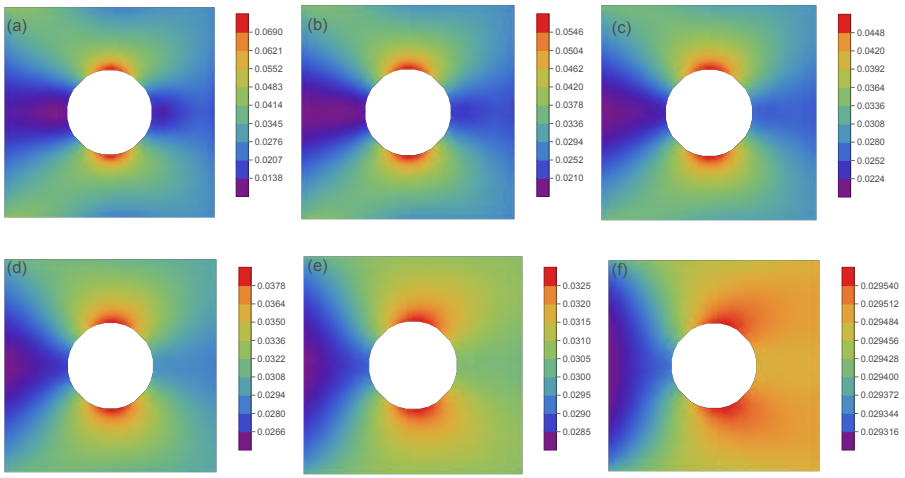

Figure 11: $\frac{\partial u}{\partial X}$ distribution based on E^1 elasticity for (a) $l_1 = 0.05$, (b) $l_1 = 0.1$, (c) $l_1 = 0.15$, (d) $l_1 = 0.25$, (e) $l_1 = 0.5$, (f) $l_1 = 2.5$.

5.5. Large deformation of 2D plate with a hole

Again, we adopt the material parameters and plate dimensions from the previous example and study the deformation of a 2D plate with a hole based on E^n elasticity, with

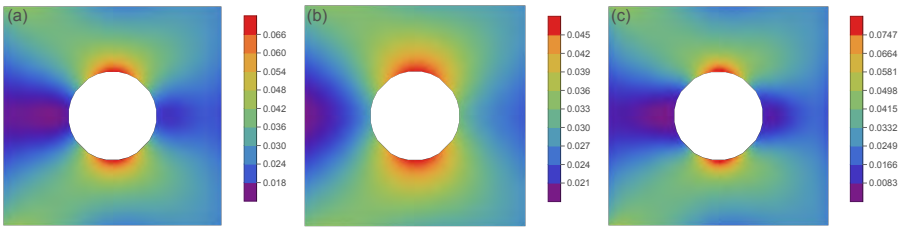

Figure 12: $\frac{\partial u}{\partial X}$ distribution based on E^2 elasticity for (a) $l_1 = l_2 = 0.05$, (b) $l_1 = l_2 = 0.1$, (c) $l_1 = l_2 = 0.025$.

n=(0,1,2,3,4,5). The geometry and boundary conditions are illustrated in Fig.3(c). The plate is discretized into 81x81 particles and the particles in the hole are removed. A shear load $p = T$ GPa·m, where $T \in [0, 3]$ is the time step, is applied on the right side boundary of the plate. The length scales are selected as $l_1 = l_2 = 0.05$ for E^2 elasticity, $l_1 = l_2 = l_3 = l_4 = 0.05$ for E^4 elasticity and $l_1 = l_2 = l_3 = l_4 = l_5 = 0.05$ for E^5 elasticity. The displacements at step $T = 1$ are plotted in Fig.13, where E^0 elasticity has the largest deformation and the deformations by E^2, E^3, E^4, E^5 elasticity are similar.

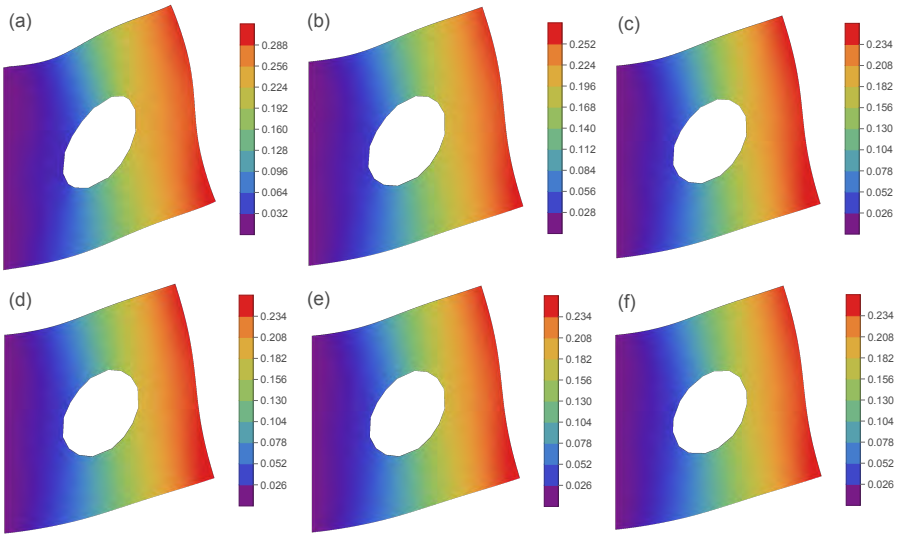

Figure 13: The deformations of the plate at $T = 1$ for (a) E^0 elasticity,(b) E^1 elasticity,(c) E^2 elasticity,(d) E^3 elasticity,(e) E^4 elasticity and (f) E^5 elasticity, respectively. Unit:meters.

Fig.14 shows that the displacement in y-direction of particle on the bottom line (e.g. the blue line in Fig.3(c)). It can be seen that the higher order gradient theory has smaller deformation. The difference becomes smaller when the order of gradient elasticity increases.

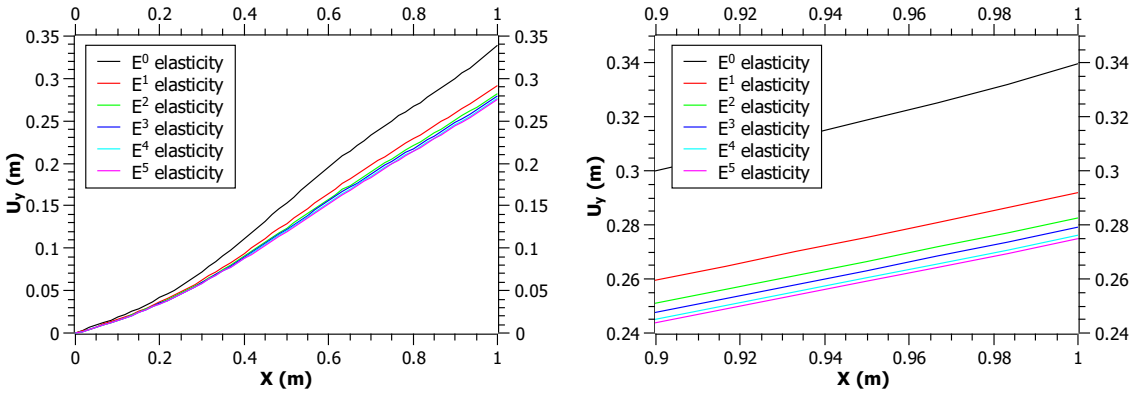

(a) (b)

Figure 14: The displacement in y-direction of all particles on the right side boundary of the plate with load level $T = 1$, where the lines in (b) are magnified from (a).

Contour plots of displacement gradients for $E^0, ..., E^5$ elasticity are plotted in Fig.15 and Fig.16. Higher order elasticity exhibits a very smooth displacement gradient. The gradient of the displacement field for hyperelasticity (E^0 elasticity) is not smooth around the internal line. This is due to the fact that the first order NOM is used, which is continuous in the displacement but discontinuous in its derivative.

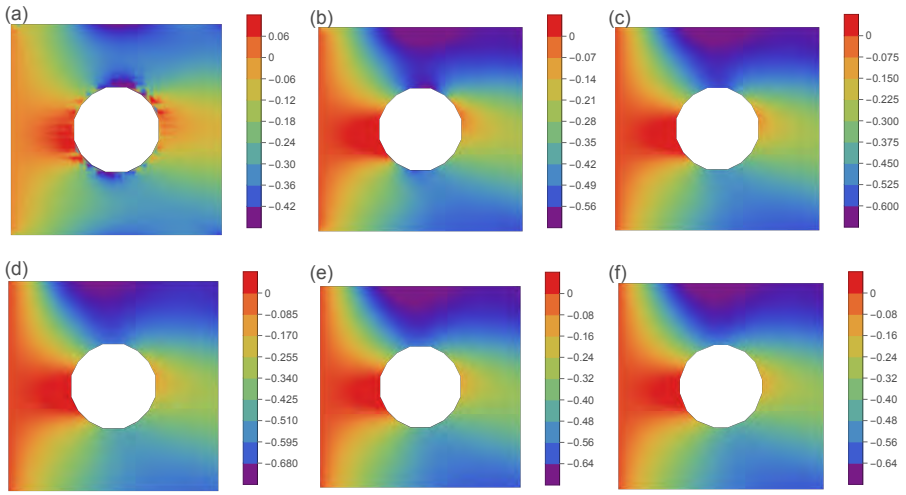

Figure 15: $\frac{\partial u}{\partial Y}$ at $T = 1$ for $E^0, ..., E^5$ elasticity.

Although the deformations for different elasticity theories at $T = 1$ are similar, the final

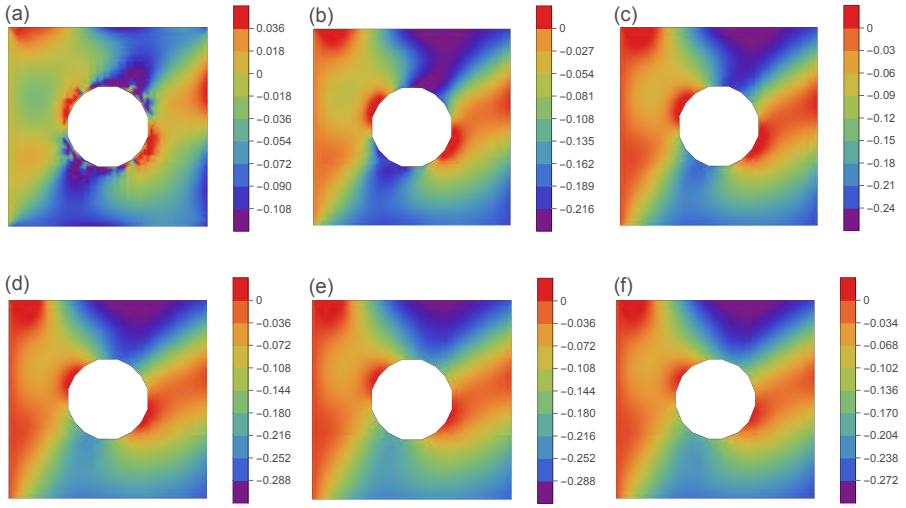

Figure 16: $\frac{\partial v}{\partial Y}$ at $T = 1$ for $E^0, ..., E^5$ elasticity.

converged deformations are different. The final load level of the plate occurs approximately at $T_0 = 0.96875, T_1 = 2.0, T_2 = 2.25, T_3 = 2.5, T_4 = 2.5, T_5 = 2.5$ for $E^0, E^1, ..., E^5$ elasticity, respectively. The final configurations of the plate can be found in Fig.17. The displacement in y-direction for particles on the right side of the plate is depicted in Fig.18

5.6. Large deformation of 3D plate subjected to line load

Finally, we present a large deformation example in 3D, i.e. a 3D thick plate based on E^3 elasticity. The geometry and boundary conditions are depicted in Fig.3(d). The particles in the red segment are fixed in all directions. A line force density of $p = 10^8$ N/m is applied on the particles located on the line. The load level T increases from 0 to 3. The differential operators in 3D E^3 elasticity are given in Eq.80. The plate with dimensions of $1 \times 1 \times 0.2\, m^3$ is discretized into $41 \times 41 \times 9 = 15129$ particles. The support of each particle consists of 124 nearest neighbors. The material parameters from the previous examples are adopted. The length scale parameters are selected as $l_1 = l_2 = l_3 = 0.05$. The final deformation is plotted in Fig.19 with the displacement fields shown in each sub-figure. The displacement gradient fields are plotted in Fig.20. The displacement second-gradient fields are plotted in Fig.21.

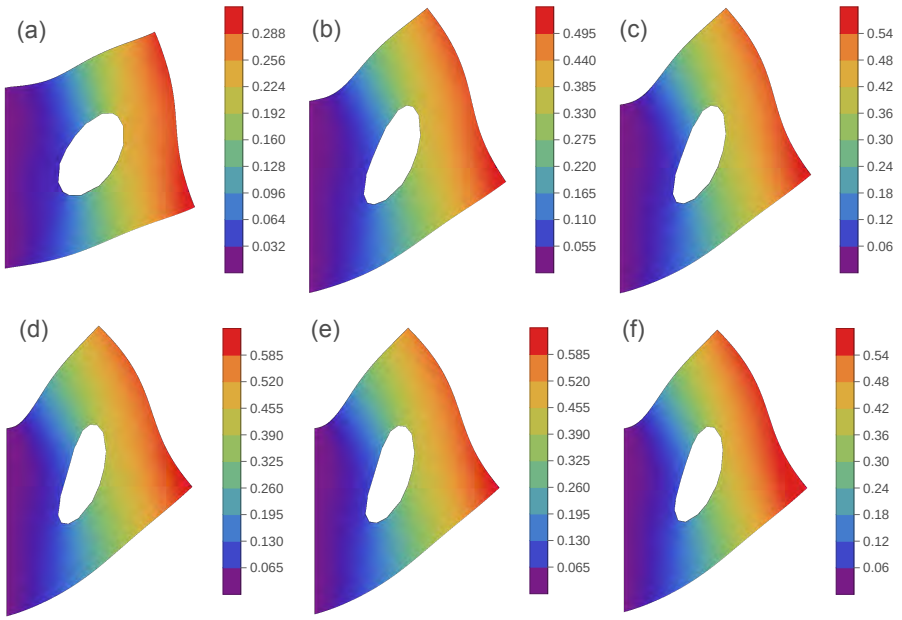

Figure 17: The converged final deformations of plate for (a) E^0 elasticity,(b) E^1 elasticity,(c) E^2 elasticity,(d) E^3 elasticity,(e) E^4 elasticity and (f) E^5 elasticity, respectively.

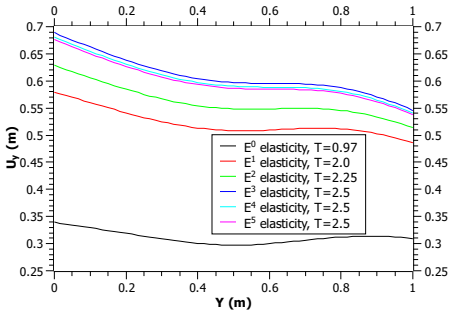

Figure 18: The displacement in y-direction for particles on the right side of the plate (i.e.red line in Fig.3(c)). Units:meters.

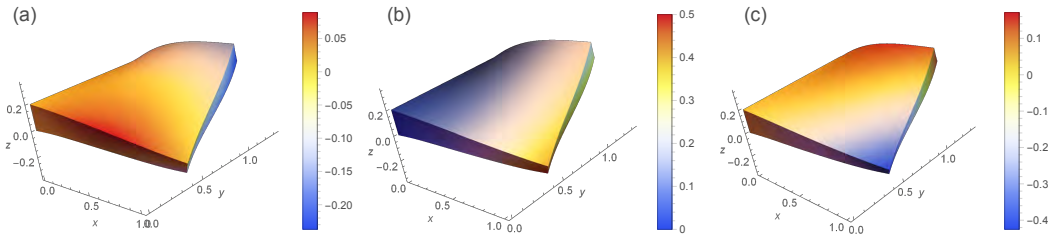

Figure 19: The displacement field of (x, y, z) directions in deformed configuration. Unit:meters.

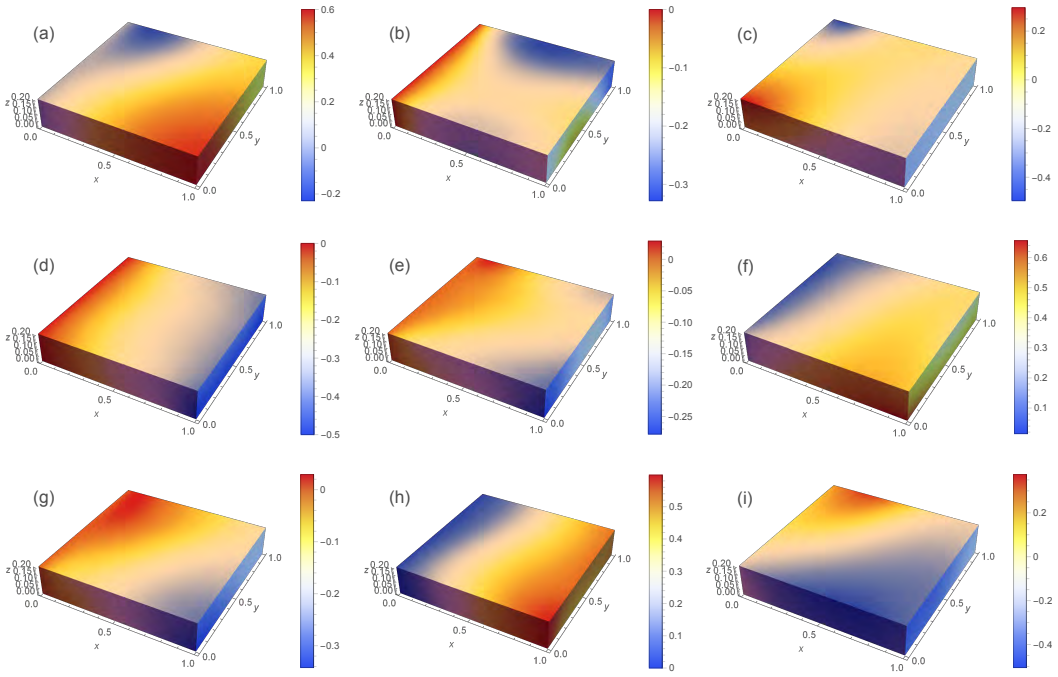

Figure 20: The gradient of displacement field (a) $\frac{\partial u}{\partial Z}$,(b) $\frac{\partial u}{\partial Y}$, (c) $\frac{\partial u}{\partial X}$, (d) $\frac{\partial v}{\partial Z}$, (e) $\frac{\partial v}{\partial Y}$, (f) $\frac{\partial v}{\partial X}$, (g) $\frac{\partial w}{\partial Z}$, (h) $\frac{\partial w}{\partial Y}$, (i) $\frac{\partial w}{\partial X}$.

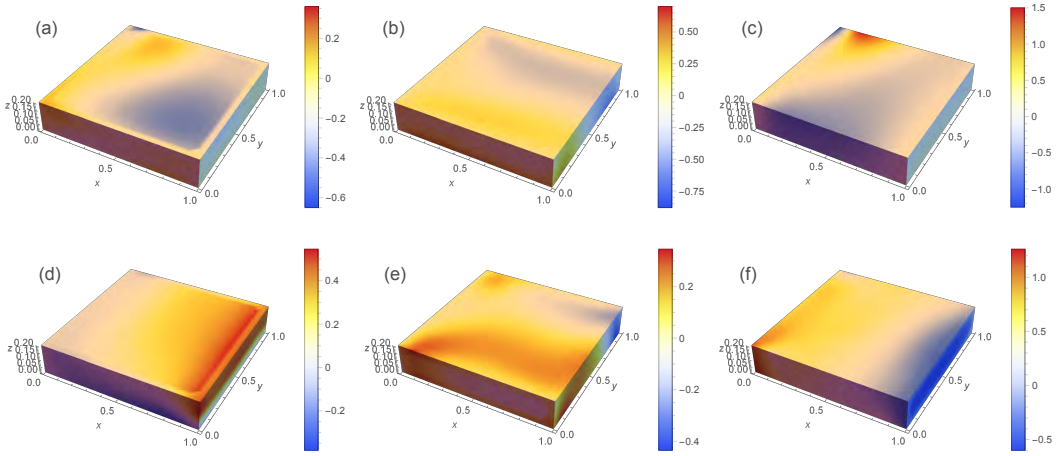

Figure 21: The second-order derivatives of displacement field (a) $\frac{\partial^2 u}{\partial Z^2}$, (b) $\frac{\partial^2 u}{\partial Y^2}$, (c) $\frac{\partial^2 u}{\partial X^2}$, (d) $\frac{\partial^2 v}{\partial Z^2}$, (e) $\frac{\partial^2 v}{\partial Y^2}$,(f) $\frac{\partial^2 v}{\partial X^2}$.

6. Conclusions

We have proposed an objective energy functional for finite deformation higher order gradient elasticity. The energy functional is based on the setting of the second Piola-Kirchhoff stress which is invariant under rigid body transformations. More specifically, the geometric nonlinear higher order gradient elasticity theory is formulated on the gradients of the right Cauchy Green tensor. The general form of higher order gradient elasticity may contain thousands of material parameters and we proposed a simplified version of gradient elasticity. Such simplification reduces the number of material parameters from 10 thousands to less than 10. A small number of material parameters can greatly simplify the experiment measurement and numerical implementation. The framework of gradient elasticity also allows for other forms of simplification of material parameters. We employed the nonlocal local operator method and Newton Raphson iteration method to find the numerical solution of higher gradient elasticity. The properties of gradient elasticity are studied by a series of numerical experiments. The numerical tests show that gradient elasticity can sustain point/line load without stress singularity. The mechanical response greatly depends on the internal length scales of gradient elasticity. Larger internal length scale induces a smaller and smoother deformation. Higher order gradient elasticity is numerically more stable and allows for larger ultimate load for the same structure. In the next stage, more physics-related research including the calibration of material parameters by experiments and numerical simulation, and the size effect, surface effect in metamaterials and gradient elasticity will be pursued. Some outlooks based on current research include, for example,

1. The higher order gradient elastoplasticity theory [32] and its numerical implementation. Current research is restricted to elasticity with finite deformation and it cannot be applied to a dissipated system involving permanent deformation or irreversible process. The extension of higher order elasticity to higher order plasticity can broaden the range of plasticity theory.

2. More clear relationship between metamaterial and gradient elasticity is expected [59, 60]. One salient feature of gradient elasticity is the micro-structure, which is essential to the

theory of metamaterials as well. Direct simulation of micro-structure requires tremendous computer power. Gradient elasticity circumvents these difficulties by introducing certain internal length scales, which however require more sophisticated measurement.

3. The wave propagation analysis of gradient elasticity. Gradient elasticity has the capability to account for interesting phenomena such as size effect, surface effect and nonlocal effect. These features may give rise to some abnormal physical phenomenon, which can be exploited to design some smart devices.

Appendix A. Symmetry of higher order tensor

For the 4th-order elasticity tensor, the symmetry can significantly reduce the number of material parameters. The symmetry of the Cauchy stress tensor ($\sigma_{ij} = \sigma_{ji}$ and the generalized Hooke's laws ($\sigma_{ij} = C_{ijkl}\varepsilon_{kl}$) implies that $C_{ijkl} = C_{jikl}$. Similarly, the symmetry of the infinitesimal strain tensor implies that $C_{ijkl} = C_{ijlk}$. These symmetries are called the minor symmetries

If in addition, since the displacement gradient and the Cauchy stress are work conjugate, the stress–strain relation can be derived from a strain energy density functional (U), then

$$\sigma_{ij} = \frac{\partial U}{\partial \varepsilon_{ij}} \quad \Longrightarrow \quad C_{ijkl} = \frac{\partial^2 U}{\partial \varepsilon_{ij} \partial \varepsilon_{kl}}. \tag{A.1}$$

The arbitrariness of the order of differentiation implies that $C_{ijkl} = C_{klij}$.

The stiffness matrix $\boldsymbol{C}$ satisfies a given symmetry condition if it does not change when subjected to the corresponding orthogonal transformation, which may represent symmetry with respect to a point, an axis, or a plane.

According to [61, 62], the orthogonal transformation of a tensor of any order can be written as

$$T(\boldsymbol{M}) := (\boldsymbol{Q} \star \boldsymbol{M})_{\ldots ijk \ldots} = \cdots Q_{ip} Q_{jq} Q_{kr} \cdots M_{\ldots pqr \ldots} \tag{A.2}$$

where $\boldsymbol{Q}$ is an orthogonal matrix given by

$$\mathbb{O}(n, R) = \left\{ \boldsymbol{Q} \in \mathrm{GL}(n, R) | \boldsymbol{Q}^T \boldsymbol{Q} = \boldsymbol{Q} \boldsymbol{Q}^T = \boldsymbol{I} \right\}, \tag{A.3}$$

with $\mathrm{GL}(n, R)$ being the set of all real $n \times n$ matrices and $\boldsymbol{I}$ the identity matrix.

The symmetry of certain orthogonal transformation of a tensor requires

$$\boldsymbol{Q} \star \boldsymbol{M} = \boldsymbol{M}, \text{ with } \boldsymbol{Q} \in \mathbb{O}(n, R). \tag{A.4}$$

The common orthogonal transformations in 3D include the reflection, rotation. The transformation matrices for symmetry planes are

$$\boldsymbol{A}_1 = \begin{bmatrix} -1 & 0 & 0 \\ 0 & 1 & 0 \\ 0 & 0 & 1 \end{bmatrix}, \boldsymbol{A}_2 = \begin{bmatrix} 1 & 0 & 0 \\ 0 & -1 & 0 \\ 0 & 0 & 1 \end{bmatrix}, \boldsymbol{A}_3 = \begin{bmatrix} 1 & 0 & 0 \\ 0 & 1 & 0 \\ 0 & 0 & -1 \end{bmatrix} \tag{A.5}$$

Rotation matrix in 3D

$$R_x(\theta) = \begin{bmatrix} 1 & 0 & 0 \\ 0 & \cos\theta & -\sin\theta \\ 0 & \sin\theta & \cos\theta \end{bmatrix}, R_y(\theta) = \begin{bmatrix} \cos\theta & 0 & \sin\theta \\ 0 & 1 & 0 \\ -\sin\theta & 0 & \cos\theta \end{bmatrix}, R_z(\theta) = \begin{bmatrix} \cos\theta & -\sin\theta & 0 \\ \sin\theta & \cos\theta & 0 \\ 0 & 0 & 1 \end{bmatrix} \tag{A.6}$$

The general rotation matrix R can be written as

$$R = R_z(\alpha)\, R_y(\beta)\, R_x(\gamma)$$

The coordinate transform of a vector in matrix and tensor notation is

$$\boldsymbol{v}' = \boldsymbol{Q} \cdot \boldsymbol{v} \qquad \text{and} \qquad v_i' = \lambda_{ij} v_j \tag{A.7}$$

The coordinate transform of a tensor in matrix and tensor notation is

$$\boldsymbol{\sigma}' = \boldsymbol{Q} \cdot \boldsymbol{\sigma} \cdot \boldsymbol{Q}^T \qquad \text{and} \qquad \sigma_{mn}' = \lambda_{mi} \lambda_{nj} \sigma_{ij} \tag{A.8}$$

The coordinate transform of a 4th-order tensor is

$$\boldsymbol{C}' = \boldsymbol{Q} \cdot \boldsymbol{Q} \cdot \boldsymbol{C} \cdot \boldsymbol{Q}^T \cdot \boldsymbol{Q}^T, C_{ijkl}' = \lambda_{im} \lambda_{jn} \lambda_{ko} \lambda_{lp} C_{mnop} \tag{A.9}$$

The coordinate transform of a 6th-order tensor is

$$\boldsymbol{H}' = \boldsymbol{Q}\cdot\boldsymbol{Q}\cdot\boldsymbol{Q}\cdot\boldsymbol{H}\cdot\boldsymbol{Q}^T\cdot\boldsymbol{Q}^T\cdot\boldsymbol{Q}^T, H'_{ijklmn} = \lambda_{io}\lambda_{jp}\lambda_{kq}\lambda_{lr}\lambda_{ms}\lambda_{nt}H_{opqrst} \tag{A.10}$$

Solving Eqs .A.9,A.10 by Mathematica [57], we can obtain the independent variables in high order tensor.

There are $3^6 = 729$ terms in $\boldsymbol{H}$. The Minor symmetry reduces $\boldsymbol{H}$ into 171 independent terms.

The orthotropy requires $\boldsymbol{H}' = \boldsymbol{H}, \boldsymbol{C}' = \boldsymbol{C}$ for three reflection symmetries $\boldsymbol{A}_1, \boldsymbol{A}_2, \boldsymbol{A}_3$. The case of orthotropy (the symmetry of a brick) has 51 independent elements.

The isotropy property requires $\boldsymbol{H}' = \boldsymbol{H}, \boldsymbol{C}' = \boldsymbol{C}$ for any rotation. This requirement reduces the number of independent terms in $\boldsymbol{H}'$ from 171 to 5.

Appendix B. Matrix Form of strain gradient energy by Viogt notations

The tensor form of higher order tensor contains many repeated terms when symmetry property is considered. In terms of numerical implementation, it is more convenient to use the matrix form than to use tensor form. In conventional mechanics, the Voigt notation is an efficient method to formulate the matrix form. Let us take the strain gradient linear elasticity for an example. The other higher order tensor can be formulated in the same manner. The material constitutive for couple-stresses can be written as

$$\overrightarrow{\nabla\sigma} = \mathcal{H}\overrightarrow{\nabla\varepsilon}, \quad \sigma_{ijk} = h_{ijklmn}\varepsilon_{lmn} \tag{B.1}$$

The strain-gradient energy function is

$$\mathcal{F} = \frac{1}{2}\sigma_{ijk}\varepsilon_{ijk} = \frac{1}{2}\varepsilon_{ijk}h_{ijklmn}\varepsilon_{lmn} = \frac{1}{2}\overrightarrow{\nabla\boldsymbol{\varepsilon}}^T\mathcal{H}\overrightarrow{\nabla\boldsymbol{\varepsilon}} \tag{B.2}$$

where $\varepsilon_{ijk}, \sigma_{ijk}$ are defined as

$$\varepsilon_{ijk} = \frac{\partial\varepsilon_{jk}}{\partial x_i}, \quad \sigma_{ijk} = \frac{\partial\sigma_{jk}}{\partial x_i}. \tag{B.3}$$

The vectorial forms of couple stress and strain gradient can be written as

$$\begin{aligned}\overrightarrow{\nabla\boldsymbol{\sigma}} = (&\sigma_{111},\sigma_{122},\sigma_{133},\sigma_{123},\sigma_{113},\sigma_{112},\sigma_{211},\sigma_{222},\sigma_{233},\\ &\sigma_{223},\sigma_{213},\sigma_{212},\sigma_{311},\sigma_{322},\sigma_{333},\sigma_{323},\sigma_{313},\sigma_{312})\end{aligned} \tag{B.4}$$

$$\overrightarrow{\nabla\boldsymbol{\varepsilon}} = (\varepsilon_{111}, \varepsilon_{122}, \varepsilon_{133}, 2\varepsilon_{123}, 2\varepsilon_{113}, 2\varepsilon_{112}, \varepsilon_{211}, \varepsilon_{222}, \varepsilon_{233},$$
$$2\varepsilon_{223}, 2\varepsilon_{213}, 2\varepsilon_{212}, \varepsilon_{311}, \varepsilon_{322}, \varepsilon_{333}, 2\varepsilon_{323}, 2\varepsilon_{313}, 2\varepsilon_{312}) \tag{B.5}$$

Based on Voigt rotations

$$\begin{array}{cccccccc} ij & =11 & 22 & 33 & 23,32 & 13,31 & 12,21 \\ \Downarrow & \Downarrow & \Downarrow & \Downarrow & \Downarrow & \Downarrow & \Downarrow \\ \alpha & =1 & 2 & 3 & 4 & 5 & 6 \end{array} \tag{B.6}$$

we write the couple stress and strain gradient as

$$\epsilon_{i\alpha} = \frac{\partial \varepsilon_\alpha}{\partial x_i}, \quad \sigma_{i\alpha} = \frac{\partial \sigma_\alpha}{\partial x_i} \tag{B.7}$$

$$h_{ijklmn} \to h_{i\alpha l\beta} \tag{B.8}$$

where α, β are the Voigt notations of jk and mn, respectively.

Then the vectorial forms of couple stress and strain gradient can be written as

$$\overrightarrow{\nabla\boldsymbol{\epsilon}} = (\epsilon_{11}, \epsilon_{12}, \epsilon_{13}, 2\epsilon_{14}, 2\epsilon_{15}, 2\epsilon_{16}, \epsilon_{21}, \epsilon_{22}, \epsilon_{23}, 2\epsilon_{24}, 2\epsilon_{25}, 2\epsilon_{26}, \epsilon_{31}, \epsilon_{32}, \epsilon_{33}, 2\epsilon_{34}, 2\epsilon_{35}, 2\epsilon_{36}) \tag{B.9}$$

$$\overrightarrow{\nabla\boldsymbol{\sigma}} = (\sigma_{11}, \sigma_{12}, \sigma_{13}, \sigma_{14}, \sigma_{15}, \sigma_{16}, \sigma_{21}, \sigma_{22}, \sigma_{23}, \sigma_{24}, \sigma_{25}, \sigma_{26}, \sigma_{31}, \sigma_{32}, \sigma_{33}, \sigma_{34}, \sigma_{35}, \sigma_{36}) \tag{B.10}$$

Based on the symmetry calculation in Appendix A, the matrix form of isotropic gradient elasticity can be derived accordingly.

References

[1] E Cosserat and F Cosserat. Théorie des corps déformables. 1909.

[2] R D Mindlin and N N Eshel. On first strain-gradient theories in linear elasticity. *International Journal of Solids and Structures*, 4(1):109–124, 1968.

[3] R D Mindlin. Micro-structure in linear elasticity. *Arch. Ration. Mech. Anal.*, 16:51–78, Jan 1964.

[4] A C Eringen. On differential equations of nonlocal elasticity and solutions of screw dislocation and surface waves. *J. Appl. Phys.*, 54(9):4703–4710, Sep 1983.

[5] R A Toupin. Elastic materials with couple-stresses. *Arch. Ration. Mech. Anal.*, 11(1):385–414, Jan 1962.

[6] R A Toupin. Theories of elasticity with couple-stress. *Arch. Ration. Mech. Anal.*, 17(2):85–112, Jan 1964.

[7] A R Hadjesfandiari and G F Dargush. Boundary element formulation for plane problems in couple stress elasticity. *International Journal for Numerical Methods in Engineering*, 89(5):618–636, 2012.

[8] F Yang, A C M Chong, D C C Lam, and P Tong. Couple stress based strain gradient theory for elasticity. *Int. J. Solids Struct.*, 39(10):2731–2743, May 2002.

[9] G C Tsiatas. A new Kirchhoff plate model based on a modified couple stress theory. *International Journal of Solids and Structures*, 46(13):2757–2764, 2009.

[10] C Polizzotto. A gradient elasticity theory for second-grade materials and higher order inertia. *International Journal of Solids and Structures*, 49(15-16):2121–2137, 2012.

[11] P Müller and A Saúl. Elastic effects on surface physics. *Surface Science Reports*, 54(5-8):157–258, 2004.

[12] FD Fischer, T Waitz, D Vollath, and NK Simha. On the role of surface energy and surface stress in phase-transforming nanoparticles. *Progress in Materials Science*, 53(3):481–527, 2008.

[13] D Davydov, A Javili, and P Steinmann. On molecular statics and surface-enhanced continuum modeling of nano-structures. *Computational Materials Science*, 69:510–519, 2013.

[14] R Artan and T Yelkenci. Rectangular rigid stamp on a nonlocal elastic half-plane. *International journal of solids and structures*, 33(24):3577–3586, 1996.

[15] ZG Zhou, JC Han, and SY Du. Investigation of a griffith crack subject to anti-plane shear by using the non-local theory. *International Journal of Solids and Structures*, 36(26):3891–3901, 1999.

[16] JC Reiher, I Giorgio, and A Bertram. Finite-element analysis of polyhedra under point and line forces in second-strain gradient elasticity. *Journal of Engineering Mechanics*, 143(2):04016112, 2017.

[17] PV Yudin and AK Tagantsev. Fundamentals of flexoelectricity in solids. *Nanotechnology*, 24(43):432001, 2013.

[18] KM Hamdia, H Ghasemi, XY Zhuang, N Alajlan, and T Rabczuk. Sensitivity and uncertainty analysis for flexoelectric nanostructures. *Computer Methods in Applied Mechanics and Engineering*, 337:95–109, 2018.

[19] XY Zhuang, BH Nguyen, SS Nanthakumar, Thai Q Tran, N Alajlan, and T Rabczuk. Computational modeling of flexoelectricity—a review. *Energies*, 13(6):1326, 2020.

[20] Y Yang and A Misra. Micromechanics based second gradient continuum theory for shear band modeling in cohesive granular materials following damage elasticity. *International Journal of Solids and Structures*, 49(18):2500–2514, 2012.

[21] A Rodríguez-Ferran, T Bennett, H Askes, and E Tamayo-Mas. A general framework for softening regularisation based on gradient elasticity. *International Journal of Solids and Structures*, 48(9):1382–1394, 2011.

[22] L Placidi, E Barchiesi, and A Misra. A strain gradient variational approach to damage: a comparison with damage gradient models and numerical results. *Mathematics and Mechanics of Complex Systems*, 6(2):77–100, 2018.

[23] D Del Vescovo and I Giorgio. Dynamic problems for metamaterials: review of existing models and ideas for further research. *International Journal of Engineering Science*, 80:153–172, 2014.

[24] S Papargyri-Beskou and D Beskos. Static analysis of gradient elastic bars, beams, plates and shells. *Open Mechanics Journal*, 4:65–73, 2010.

[25] H Askes and EC Aifantis. Gradient elasticity and flexural wave dispersion in carbon nanotubes. *Physical Review B*, 80(19):195412, 2009.

[26] RD Mindlin. Second gradient of strain and surface-tension in linear elasticity. *International Journal of Solids and Structures*, 1(4):417–438, 1965.

[27] C Polizzotto. A second strain gradient elasticity theory with second velocity gradient inertia–part i: Constitutive equations and quasi-static behavior. *International Journal of Solids and Structures*, 50(24):3749–3765, 2013.

[28] C Polizzotto. A second strain gradient elasticity theory with second velocity gradient inertia–part ii: Dynamic behavior. *International Journal of Solids and Structures*, 50(24):3766–3777, 2013.

[29] H Askes, ASJ Suiker, and LJ Sluys. A classification of higher-order strain-gradient models–linear analysis. *Archive of Applied Mechanics*, 72(2-3):171–188, 2002.

[30] A Javili, F dell'Isola, and P Steinmann. Geometrically nonlinear higher-gradient elasticity with energetic boundaries. *Journal of the Mechanics and Physics of Solids*, 61(12):2381–2401, 2013.

[31] JC Reiher and A Bertram. Finite third-order gradient elasticity and thermoelasticity. *Journal of Elasticity*, 133(2):223–252, 2018.

[32] JC Reiher and A Bertram. Finite third-order gradient elastoplasticity and thermoplasticity. *Journal of Elasticity*, 138(2):169–193, 2020.

[33] J Y Shu, W E King, and N A Fleck. Finite elements for materials with strain gradient effects. *International Journal for Numerical Methods in Engineering*, 44(3):373–391, 1999.

[34] E Amanatidou and N Aravas. Mixed finite element formulations of strain-gradient elasticity problems. *Computer Methods in Applied Mechanics and Engineering*, 191(15-16):1723–1751, 2002.

[35] H Askes and M A Gutiérrez. Implicit gradient elasticity. *International Journal for Numerical Methods in Engineering*, 67(3):400–416, 2006.

[36] E Atroshchenko and SPA Bordas. Fundamental solutions and dual boundary element methods for fracture in plane cosserat elasticity. *Proceedings of the Royal Society A: Mathematical, Physical and Engineering Sciences*, 471(2179):20150216, 2015.

[37] H Askes and E C Aifantis. Numerical modeling of size effects with gradient elasticity-formulation,

meshless discretization and examples. *International Journal of Fracture*, 117(4):347–358, 2002.

[38] Z Tang, S Shen, and SN Atluri. Analysis of materials with strain-gradient effects: a meshless local petrov-galerkin (mlpg) approach, with nodal displacements only. *Computer Modeling in Engineering and Sciences*, 4(1):177–196, 2003.

[39] V Balobanov, S Khakalo, and J Niiranen. Isogeometric analysis of gradient-elastic 1d and 2d problems. In *Generalized Continua as Models for Classical and Advanced Materials*, pages 37–45. Springer, 2016.

[40] S Khakalo and J Niiranen. Isogeometric analysis of higher-order gradient elasticity by user elements of a commercial finite element software. *Comput.-Aided Des.*, 82:154–169, Jan 2017.

[41] J Niiranen, J Kiendl, A H. Niemi, and A Reali. Isogeometric analysis for sixth-order boundary value problems of gradient-elastic Kirchhoff plates. *Computer Methods in Applied Mechanics and Engineering*, 316:328–348, Apr 2017.

[42] CL Thanh, LV Tran, T Vu-Huu, and M Abdel-Wahab. The size-dependent thermal bending and buckling analyses of composite laminate microplate based on new modified couple stress theory and isogeometric analysis. *Computer Methods in Applied Mechanics and Engineering*, 350:337–361, 2019.

[43] P Phung-Van, C H Thai, H Nguyen-Xuan, and M A Wahab. Porosity-dependent nonlinear transient responses of functionally graded nanoplates using isogeometric analysis. *Composites Part B: Engineering*, 164:215–225, 2019.

[44] H X Nguyen, T N Nguyen, M Abdel-Wahab, SPA Bordas, H Nguyen-Xuan, and T P Vo. A refined quasi-3d isogeometric analysis for functionally graded microplates based on the modified couple stress theory. *Computer Methods in Applied Mechanics and Engineering*, 313:904–940, 2017.

[45] HL Ren, XY Zhuang, and T Rabczuk. Nonlocal operator method with numerical integration for gradient solid. *Computers & Structures*, 233:106235, 2020.

[46] HL Ren, XY Zhuang, and T Rabczuk. A higher order nonlocal operator method for solving partial differential equations. *Computer Methods in Applied Mechanics and Engineering*, 367:113132, 2020.

[47] HL Ren, XY Zhuang, and T Rabczuk. A nonlocal operator method for solving partial differential equations. *Computer Methods in Applied Mechanics and Engineering*, 358:112621, 2020.

[48] HL Ren, XY Zhuang, YC Cai, and T Rabczuk. Dual-horizon peridynamics. *International Journal for Numerical Methods in Engineering*, 2016.

[49] HL Ren, XY Zhuang, and T Rabczuk. Dual-horizon peridynamics: A stable solution to varying horizons. *Computer Methods in Applied Mechanics and Engineering*, 318:762–782, 2017.

[50] S A Silling. Reformulation of elasticity theory for discontinuities and long-range forces. *Journal of the Mechanics and Physics of Solids*, 48(1):175–209, 2000.

[51] S A Silling, M Epton, O Weckner, J Xu, and E Askari. Peridynamic states and constitutive modeling. *Journal of Elasticity*, 88(2):151–184, 2007.

[52] T Rabczuk, HL Ren, and XY Zhuang. A nonlocal operator method for partial differential equations with application to electromagnetic waveguide problem. *Computers, Materials & Continua 59 (2019), Nr. 1*, 2019.

[53] J Bonet and R D Wood. *Nonlinear continuum mechanics for finite element analysis*. Cambridge university press, 1997.

[54] J Korelc and P Wriggers. *Automation ofFinite Element Methods*. Springer, 2016.

[55] M E Gurtin and A I Murdoch. A continuum theory of elastic material surfaces. *Archive for rational mechanics and analysis*, 57(4):291–323, 1975.

[56] SP Shen and SL Hu. A theory of flexoelectricity with surface effect for elastic dielectrics. *Journal of the Mechanics and Physics of Solids*, 58(5):665–677, 2010.

[57] S Wolfram et al. *The MATHEMATICA® book, version 4*. Cambridge university press, 1999.

[58] R Makvandi, JC Reiher, A Bertram, and D Juhre. Isogeometric analysis of first and second strain gradient elasticity. *Computational Mechanics*, 61(3):351–363, 2018.

[59] S Khakalo, V Balobanov, and J Niiranen. Modelling size-dependent bending, buckling and vibrations of 2d triangular lattices by strain gradient elasticity models: applications to sandwich beams and auxetics. *International Journal of Engineering Science*, 127:33–52, 2018.

[60] H Yang, D Timofeev, I Giorgio, and W H Müller. Effective strain gradient continuum model of metamaterials and size effects analysis. *Continuum Mechanics and Thermodynamics*, pages 1–23, 2020.

[61] S Forte and M Vianello. Symmetry classes for elasticity tensors. *J. Elast.*, 43(2):81–108, May 1996.

[62] G Geymonat and T Weller. Classes de symétrie des solides piézoélectriques. *Comptes Rendus Mathematique*, 335(10):847–852, 2002.